FGF10 promotes cardiac repair through a dual cellular mechanism increasing cardiomyocyte renewal and inhibiting fibrosis

Fabien Hubert, Sandy Payan, Edeline Pelce, Laetitia Bouchard, Rachel Sturny, Nicolas Lenfant, Giovanna Mottola, Frédéric Collart, Robert Kelly, Francesca Rochais

CVR-2021-0222

FGF10 promotes cardiac repair through a dual cellular mechanism increasing cardiomyocyte renewal and inhibiting fibrosis

Fabien Hubert PhD [1#], Sandy M Payan PhD [1#], Edeline Pelce MD-MSc [1,2], Laetitia Bouchard MSc [1], Rachel Sturny [3], Nicolas Lenfant PhD [1], Giovanna Mottola PhD [4,5], Frédéric Collart MD [2], Robert G Kelly PhD [3] and Francesca Rochais PhD [1]

[1] Aix Marseille Univ, INSERM, MMG, U 1251, Marseille, France.

[2] Department of Cardiac Surgery, Timone Hospital, AP-HM, Marseille, France.

[3] Aix Marseille Univ, CNRS UMR 7288, IBDM, Marseille, France.

[4] Aix-Marseille Univ, C2VN, INSERM 1263, INRAE 1260, Marseille, France.

[5] Laboratory of Biochemistry, Timone Hospital, Marseille, France.

# These authors contributed equally

Address for correspondence

Dr. Francesca Rochais, Aix Marseille Université, MMG U1251

27 Boulevard Jean Moulin, 13005 Marseille, France

Phone : +334 91 32 48 86 ; FAX : +334 91 79 72 27

francesca.rochais@univ-amu.fr

Short Title: FGF10 promotes cardiac repair and regeneration

Original Article

Total word count: 8397

ABSTRACT

Aims. Promoting cardiomyocyte renewal represents a major therapeutic approach for heart regeneration and repair. Our study aims to investigate the relevance of FGF10 as a potential target for heart regeneration.

Methods and Results. Our results first reveal that *Fgf10* levels are upregulated in the injured ventricle after MI. Adult mice with reduced *Fgf10* expression subjected to MI display impaired cardiomyocyte proliferation and enhanced cardiac fibrosis, leading to a worsened cardiac function and remodeling post-MI. In contrast, conditional *Fgf10* overexpression post-MI revealed that, by enhancing cardiomyocyte proliferation and preventing scar-promoting myofibroblast activation, FGF10 preserves cardiac remodeling and function. Moreover, FGF10 activates major regenerative pathways including the regulation of *Meis1* expression levels, the Hippo signaling pathway and a pro-glycolytic metabolic switch. Finally, we demonstrate that elevated *FGF10* levels in failing human hearts correlate with reduced fibrosis and enhanced cardiomyocyte proliferation.

Conclusions. Altogether, our study shows that FGF10 promotes cardiac regeneration and repair through two cellular mechanisms: elevating cardiomyocyte renewal and limiting fibrosis. This study thus identifies FGF10 as a clinically relevant target for heart regeneration and repair in man.

1. INTRODUCTION

Ischemic heart disease is the leading cause of cardiovascular disease death worldwide (1). Myocardial infarction is characterized by dramatic cardiomyocyte loss associated with profound fibrotic scarring and leads to severe impairment of cardiac function and ultimately to congestive heart failure. The existence, in the adult mammalian heart, of low but detectable cardiomyocyte proliferative capacities (2) has oriented regenerative medicine toward new therapeutical strategies. Indeed, the stimulation of terminally differentiated cardiomyocyte proliferation currently represents the main therapeutic approach for heart regeneration (3). Increasing evidence demonstrating that the loss of mammalian cardiomyocyte renewal potential shortly after birth causes the loss of regenerative capacities, strongly support the hypothesis that a detailed understanding of the regulation of fetal cardiomyocyte proliferation is essential to identify targets for cardiac regeneration (4, 5). Cardiac regeneration is a complex process in which, in addition to promoting cardiomyocyte proliferation, preventing mature scar formation is essential. Interestingly, recent evidence investigating endogenous regenerative capacities in lower vertebrates suggests that reducing the fibroblast to myofibroblast transition may result in a softer scar tissue, more compliant to cardiomyocyte renewal and favorable to regeneration (6).

We recently uncovered a role for Fibroblast Growth Factor FGF10 signaling in regulating fetal cardiomyocyte proliferation (7). FGF10 is a paracrine FGF family member and is known to play essential roles in the development of multiple organs (8). *Fgf10* is expressed in second heart field (SHF) cardiac progenitor cells in the early embryo, however it is not essential for SHF deployment and subsequent heart tube elongation (9). In contrast, in the fetal heart, FGF10 controls regionalized cardiomyocyte proliferation through a cell-type autonomous

mechanism involving FOXO3 transcription factor phosphorylation and subsequent downregulation of the cyclin dependent kinase inhibitor $p27^{kip1}$ expression. As a result, *Fgf10*-null embryos, which die at birth due to lung aplasia, display altered heart morphology (7, 10). Interestingly, forced *Fgf10* expression in adult mice specifically promotes cardiomyocyte cell cycle reentry (7) suggesting that FGF10 may be a potential target to improve the limited innate regenerative capacities of the myocardium after injury. In this study, using an experimental mouse model of myocardial infarction (MI) together with *Fgf10*-gain and loss of function mouse models, we demonstrate that upregulation of *Fgf10* promotes cardiac regeneration and repair post-MI. Our results reveal that this effect is mediated through the elevation of cardiomyocyte proliferation and reduction of fibrosis. Moreover, analysis of *FGF10* expression in failing explanted human hearts revealed a strong correlation between elevated *FGF10* levels, reduced fibrosis and enhanced cardiomyocyte proliferation. Together these experiments identify FGF10 as a potential clinical target to enhance cardiac repair and regeneration.

2. METHODS

2.1 Mice

Animal studies were performed according to the guidelines from Directive 2010/63/EU of the European Parliament on the protection of animals used for scientific purposes. Mouse care and procedures were approved by the Departmental Direction of Veterinary Services of the French Ministry of Agriculture and the local ethics committee (APAFIS#84 74-20170 II 009244646 v2). *Fgf10*$^{+/-}$, *Fgf10-LacZ*, *Rosa-tdT*, *αMHC-MerCreMer*, *Rosa26-rtTA* and *Tet*(O)-*Fgf10* mice were maintained on mixed genetic backgrounds. Inducible expression of *Fgf10* is achieved by feeding sequentially mice with food containing doxycycline (625 mg/kg DOX, Envigo). Floxed allele recombination in adult mice was achieved by intraperitoneal tamoxifen injection at a dose per day of 2 mg/30 g for 3 days. The Phire Animal Tissue Direct PCR Kit (Life Technologies) was used to genotype transgenic mice without prior DNA Purification. Extended genotyping procedure can be found in the Supplemental Data. For cardiac tissue collection, mice were euthanized by cervical dislocation.

2.2 Human heart samples

Human tissue samples were provided by the Cardio-Thoracic Surgery Department of La Timone Hospital Marseille, in accordance with the principles outlined in the Declaration of Helsinki and with human research protocol approved by the institution under which patient informed consent was obtained. Human heart tissues were obtained from failing explanted hearts. Patient clinical features are provided in Supplemental Table 2. All patients displayed initial myocardial infarction. Samples were collected in the right ventricle, the infarcted area, border zone and remote area of the freshly explanted heart and immediately processed. All

included hearts were arising from patients displaying left ventricular ischemic cardiomyopathy with non-altered right ventricular function.

2.3 Myocardial infarction model

Adult mice (3 month-old) were sedated with a mixture of ketamine (100 mg/kg) and xylazine (10 mg/Kg) via intraperitoneal injection, and following endotracheal intubation, were artificially ventilated. If necessary 1-2% isoflurane was added as maintenance anesthetic. For analgesia, buprenorphine. (0.1 mg/kg) was injected subcutaneously 30 min prior surgery. Following skin incision, lateral thoracotomy at the fourth intercostal space was performed by blunt dissection of the intercostal muscles. Under stereomicroscope control, the left anterior descending coronary artery was visualized and ligated (with 8.0 non-absorbable silk suture) 2.0 mm below the left atrium, just above the bifurcation of the left diagonal arteries. Effective ligation of the coronary artery was confirmed by whitening of the LV affected region below the ligation site. Out of 145 MI-mice, 30 were excluded due to malpositioning of the ligation. The thoracic wall and skin incisions were then sutured with 6.0 non-absorbable and 4.0 absorbable silk sutures, respectively. Mice were then warmed for several minutes until recovery.

2.4 Echocardiography

Heart function was evaluated at the CERIMED-Marseille, by transthoracic echocardiography performed on isoflurane-sedated mice using a Vevo 2100 VisualSonics. Mice were anesthetized with isoflurane in oxygen (2% for induction and 1% for maintenance) and placed on a warm pad at the supine position. All echocardiography measurements were performed in a blinded manner.

146 **2.5 Tissue processing**

147 Mouse hearts were dissected and analyzed using a Zeiss Lumar stereo dissecting microscope.
148 For X-gal staining, hearts were collected and fixed for 3 hours in 4% paraformaldehyde
149 (PFA), extensively washed in 1X PBS and stained for 12 hours at 37°C in a solution containing
150 4mg/ml of X-gal. After staining, the samples were washed in PBS, post-fixed in PFA 4% and
151 observed under a Zeiss Lumar stereomicroscope. For immunostaining and sirius red
152 staining, samples were fixed in 4% PFA for 3 hours and extensively washed in 1X PBS.
153 Paraffin embedding was performed following dehydration using a graded ethanol series
154 (50, 70, 90 and 100%), two xylene washes and three paraffin washes (Paraplast X-tra,
155 Sigma P3808). Cryopreservation was achieved by incubation of samples in a sucrose series
156 (15 and 30%) and embedding in OCT (VWR, 361603E). Infarct size was estimated using
157 ImageJ software on 6 sirius red stained sections containing the papillary muscle region and
158 based on the ratio of the length of the left ventricular infarct area showing fibrosis by the
159 total left ventricular length as described before (11). Extended immunostaining and sirius red
160 staining procedures, including antibody list, can be found in the Supplemental Data.
161 Cardiomyocyte proliferation analysis was examined using Ki67, PH3 and AURKB
162 immunofluorescence. The number of Ki67-, PH3- and AURKB-positive nuclei was counted
163 from 8-10 sections per individual heart. Measurements are the average of 5-7 independent
164 hearts for each indicated genotype and treatment.

165

166 **2.6 Quantitative Real Time PCR**

167 Total RNA was extracted using Trizol LS reagent (Life technologies). First strand cDNA was
168 synthesized using Maxima Reverse Transcriptase (Life technologies). qRT-PCR was performed
using the following primers and Luminaris qPCR SuperMix (Life technologies) and a Roche

Light Cycler 480. Each experiment was performed in duplicate and normalized to house-keeping gene. Detailed quantitative RT-PCR primers can be found in the Supplemental Data.

2.7 Biochemical Analysis of circulating protein levels

DOX-treated *Rosa26-RTTA/Tet(O)-Fgf10* were compared to CTRL-treated *Rosa26-RTTA/Tet(O)-Fgf10* infarcted mice, 5 days post-injury. Blood sample was collected into serum separator tube and the serum was coagulated at room temperature for 2 hours. The homogenates were centrifuged at 1000 g for 20 min, and the resultant supernatant was collected and stored at -20°C. Highly sensitive troponin T (TnT-hs, Elecsys®) was measured on COBAS-8000 Roche®, TnT-hs was measured using an immunological sandwich method (detection threshold: 5 pg/ml, range: 5–50 ng, intra-assay variation < 10%; intra-assay range: between 2 and 4%). Circulating FGF10 levels were assessed using Elisa assay according to the manufacturer's protocols (mouse FGF10 ELISA kit, Abbexa, abx574964), and the absorbance values were detected at 450 nm using a microplate reader. Serum levels of cardiac troponin I were addressed using western blot analysis. Equal amount of protein were subjected to SDS-PAGE. After electrophoresis, proteins were transferred to PVDF membranes and immunoblotted with Troponin I antibody (MAB1691, 1/1000). Proteins were detected by chemiluminescence using a Bio-Rad ChemiDoc analyser. Amido Black staining (Sigma 1.01167) was performed to visualize total protein. Relative densities were quantified using the ImageJ software. All data were normalized by internal controls.

2.8 Cardiomyocyte isolation and culture

Ventricular cardiomyocytes were obtained from 10 week-old *αMHC-MerCreMer/R26R-Tomato/R26R-RTTA/Tet(O)-Fgf10* males intraperitoneally injected with tamoxifen (2 mg/30 g

for 3 days) and the fed with normal (CTRL) or doxycycline (DOX) supplemented food for 5 days. Mice were anesthetized by intraperitoneal injection of a ketamine-xylazine cocktail (ketamine, 93.75 mg/kg; xylazine, 12.5 mg/kg), and the chest was opened to expose the heart. The descending aorta and inferior vena cava were cut and the heart was rapidly flushed by injection of EDTA buffer (130 mM NaCl, 5 mM KCl, 0.5 mM NaH_2PO_4, 10 mM HEPES, 10 mM glucose, 10 mM BDM, 10 mM Taurine and 5 mM EDTA adjusted to pH 7.8) in the right ventricle. Ascending aorta was clamped and the heart was immediatly transferred to a 60-mm dish containing fresh EDTA buffer. Digestion was achieved by sequential injection of EDTA buffer, perfusion buffer (130 mM NaCl, 5 mM KCl, 0.5 $MgCl_2$ adjusted to pH 7.8), and finally an enzymatic solution (perfusion buffer supplemented with collagenase 2 and 4 and protease XIV) into the left ventricle. The ventricles were separated from the atria, cut into small pieces, and triturated with a pipette to disperse cardiomyocytes. Ventricular cardiomyocytes were filtered (100 µm pore size filter) and allowed to sediment by gravity for 20 minutes. The supernatant was removed, and cells were suspended in three intermediate calcium reintroduction buffers (0.34, 0.68 and 1.02 mmol/l Ca^{2+}) to gradually restore calcium concentration to physiological levels. At the end, ventricular cardiomyocytes were resuspended in a culture medium and plated in culture dishes coated with laminin (Life Technologies, 10 µg/ml).

2.9 Cell culture and pharmacological stimulations

Human cardiac fibroblast (HCF) cell line (Promocell®, C-12375) was cultured in Fibroblast Growth Medium 3 (Promocell®, C-23025). Cells were maintained at 37°C in a 95% air-5% CO_2 humidified atmosphere, fed every 2–3 days, and sub-cultured when reaching 70–80%. HCF

were treated with TGF-β1 (Miltenyi Biotec, 5µg/ml) and recombinant FGF10 (R&D Systems, 100ng/ml).

2.10 RNA sequencing

Sequencing and bioinformatics analysis were performed by the Genomics and Bioinformatics facility (GBiM) from the U 1251/Marseille Medical Genetics. RNA-Seq was performed in quadruplicate on DOX-treated *Rosa26-RTTA/Tet(O)-Fgf10* infarcted area 21 days post-injury as compared to the same area from CTRL-treated *Rosa26-RTTA/Tet(O)-Fgf10*. Before sequencing, the quality of total RNA samples was assessed using a bioanalyzer (Agilent, Santa Clara, California, USA). Only RNAs with RNA Integrity Numbers (RIN) above 8 were used. For each sample, a library for poly(A)+ RNA was prepared from 1 µg of total RNA, using the TruSeq Stranded mRNA Library Prep kit (Illumina, San Diego, California, USA), following the manufacturer's instructions. The 8 indexed libraries were pooled and sequenced on an Illumina NextSeq 500 platform, using paired-end mode (2*75 bp reads), in order to reach 50 million reads (clusters) for each library. Detailed data processing and differential gene expression (DGE) analysis can be found in the Supplemental Data.

2.11 Statistics

All experiments and data analysis were conducted blinded. The number of replicates (n) is indicated in the figure legends and refers to the number of experimental subjects independently treated in each experimental condition. Data are presented as means ± s.e.m. Statistical significance (p) was determined using unpaired Student's *t*-test, Student's *t*-distribution and Fisher test, as indicated in each figure legend. Statistical significance was set at $*p < 0.05$, $0.001<**p < 0.01$, $***p < 0.001$.

3. RESULTS

3.1 *Fgf10* upregulation following MI

To study the role of FGF10 in ischemic heart disease, we first analyzed cardiac *Fgf10* expression in mice subjected to myocardial infarction (MI) through ligation of the left anterior descending coronary artery. 21 days after ligation, mice were sacrificed, hearts were removed and qRT-PCR experiments revealed upregulated endogenous *Fgf10* levels in the injured ventricle (Fold Change (FC)=3.5; Supplemental Figure 1A). Analysis of cryostat sections from *Fgf10-LacZ* hearts 21 days post-MI showed that X-gal^{+} nuclei are exclusively present in cardiomyocytes (data not shown), suggesting that *Fgf10* expression is upregulated in cardiomyocytes under pathological conditions. Directly controlled by key developmental transcription factors including NKX2-5, TBX1 and ISL1, a cardiac enhancer, located in the first intron of *Fgf10* gene, has been identified and described to be necessary and sufficient to direct *Fgf10* expression in the developing heart. While ISL1 and TBX1 activate *Fgf10* expression in cardiac progenitor cells, NKX2-5 mediates its repression (12). In order to address a potential involvement of NKX2-5, TBX1 and ISL1 in the upregulation of *Fgf10* expression post-MI, we evaluated *Nkx2-5*, *Tbx1* and *Isl1* expression in the injured ventricle. Interestingly, while *Nkx2-5* expression levels were downregulated (Supplemental Figure 1B), strong upregulation of *Tbx1* and *Isl1* mRNA levels was observed 21 days post-MI (Supplemental Figure 1C-D). Consistent with cardiomyocyte dedifferentiation prior to cell cycle release (13-16), our results thus suggest that reactivation of the transcriptional embryonic program may drive *Fgf10* expression under pathological conditions.

3.2 Decreased *Fgf10* dosage worsens cardiac function and remodeling following MI

In order to evaluate the role of upregulated *Fgf10* levels under pathological conditions, mice with reduced *Fgf10* expression (FC=0.56; p=0.006; WT, n=5; *Fgf10*$^{+/-}$, n=5) were subjected to MI (Figure 1A). Compared to WT-MI infarcted area, *Fgf10* expression levels in *Fgf10*$^{+/-}$-MI infarcted area 21 days post-MI were significantly reduced (FC=0.2; p=0.005; WT-MI, n=5; *Fgf10*$^{+/-}$-MI, n=6). 21 days after MI, infarct size measurement (*Fgf10*$^{+/-}$-MI: 30±8% over WT-MI, p=0.02), together with heart/body weight and heart weight/tibia length ratios (Figure 1B-C) revealed significant worsening of cardiac remodeling in *Fgf10*$^{+/-}$-MI compare to WT-MI mice. *In vivo* heart function was investigated using echocardiography (Figure 1D). Compared to WT infarcted mice, *Fgf10*$^{+/-}$ infarcted mice displayed worsened cardiac performance including a further decreased ejection fraction and fractional shortening and a further increased left ventricular volume (Figure 1E-G). Analysis of key heart failure marker expression using qRT-PCR experiments confirmed the worsened pathological remodeling in *Fgf10*$^{+/-}$-MI compare to WT-MI mice (Figure 1H). Together, these results reveal that maximal FGF10 levels play a protective role in ischemic heart failure.

3.3 Decreased *Fgf10* dosage impairs cardiomyocyte proliferation and worsens fibrosis following MI

To determine whether upregulated *Fgf10* levels in the injured ventricle could participate in cardiomyocyte renewal post-MI, cardiac cell proliferation was analyzed, in *Fgf10*$^{+/-}$-MI compare to WT-MI mice, 5 and 21 days (Figure 2A) post-MI. Immunofluorescence analysis of proliferative capacity in the border zone (BZ), using the pan-cell cycle marker Ki67 (Figure 2B-D and supplemental Figure 2A), the mitotic marker PH3 (Supplemental Figure 2B-D) and the cytokinesis marker Aurora kinase B (AURKB, Figure 2E), revealed a significant impairment of

cardiomyocyte proliferation in *Fgf10*$^{+/-}$-MI compare to WT-MI mice. Similar results were obtained when cardiomyocyte proliferation was measured in the infarcted area (IA; Supplemental Figure 2E-F). No alteration in non-myocyte proliferation capacity was detected (Supplemental Figure 2G-H). Measurement of cardiomyocyte cross-sectional area revealed that decreased *Fgf10* dosage significantly worsens cardiomyocyte hypertrophy post-MI (Figure 2F). To determine whether FGF10 haploinsufficiency impacts on the progression of cardiac fibrosis following MI, histological analysis using Sirius red staining was performed. At both 5 (Figure 2G-I) and 21 days (Figure 2J-L) post-MI, increased fibrosis was observed in *Fgf10*$^{+/-}$-MI hearts compare to WT-MI hearts, correlating with upregulated collagen gene expression (Figure 2I and L). Together, these results suggest that maximal *Fgf10* levels promote cardiomyocyte renewal and prevent fibrosis post-MI, likely contributing to preserved cardiac function and decreased remodeling.

3.4 *Fgf10* upregulation following MI preserves cardiac performance

In order to determine whether forced *Fgf10* expression after MI would promote cardiac regeneration and repair, we took an inducible gain-of-function approach. As FGF10 is a secreted molecule, global and temporal conditional overexpression of *Fgf10* was achieved using the *Rosa26-RTTA/Tet(O)-Fgf10* mouse line treated with doxycycline-supplemented (DOX) food one day after MI during 21 days (Figure 3A). *Rosa26-RTTA/Tet(O)-Fgf10* DOX-MI mice were compared with *Rosa26-RTTA/Tet(O)-Fgf10* mice treated with control food (CTRL-MI) and qRT-PCR experiments on left ventricular tissues and biochemical analysis of serum post-MI confirmed that DOX-treated mice displayed significantly upregulated myocardial (FC=106, p=7x10^{-6}, n=4 per group) and circulating *Fgf10* levels (DOX-MI: 3.1±0.2 ng/ml versus CTRL-MI: 1.9±0.2 ng/ml; p=0.007, n=4 per group). Our results demonstrated that *Fgf10*

upregulation prevents cardiac remodeling 21 days after MI, as depicted by infarct size measurement (DOX-MI: 18±4% below CTRL-MI, p=0.03), heart/body weight and heart weight/tibia length ratios (Figure 3B-C). *In vivo* heart function was investigated using echocardiography (Figure 3D). Compared to CTRL-treated *Rosa26-RTTA/Tet(O)-Fgf10* infarcted mice, DOX-treated *Rosa26-RTTA/Tet(O)-Fgf10* infarcted mice displayed preserved cardiac function and remodeling parameters including ejection fraction, fractional shortening and left ventricular dilation (Figure 3E-G). Analysis of key heart failure markers using qRT-PCR experiments confirmed the reduction of pathological remodeling in DOX-treated *Rosa26-RTTA/Tet(O)-Fgf10* infarcted mice compared to CTRL-treated *Rosa26-RTTA/Tet(O)-Fgf10* infarcted mice (Figure 3H). To confirm the specificity of the protective effect of FGF10 post-MI, *Rosa26-RTTA* transgenic mice were subjected to MI and treated with DOX-supplemented or CTRL food one day after MI during 21 days (Supplemental Figure 3A). qRT-PCR experiments performed on left ventricular tissues 21 days post-MI confirmed that DOX-treatment has no impact on myocardial *Fgf10* expression (FC=0.9±0.2, p=0.2, CTRL-*Rosa26-RTTA*-MI, DOX-*Rosa26-RTTA*-MI, n=4 per group). Similarly, no improvement in *in vivo* heart function was observed 21 days post-MI. Cardiac function and remodeling of the DOX-treated *Rosa26-RTTA*-MI mice were comparable to that of CTRL-treated *Rosa26-RTTA*-MI mice (Supplemental Figure 3), attesting to the positive effect of *Fgf10* upregulation in preserving cardiac function and reducing remodeling post-MI.

3.5 *Fgf10* upregulation following MI promotes cardiomyocyte renewal and prevents myocardial necrosis and fibrosis

To determine if endogenous *Fgf10* upregulation post-MI promotes cardiomyocyte renewal, cardiac cell proliferation was analyzed in the BZ and IA of CTRL- and DOX-treated *R26R-*

RTTA/Tet(O)-Fgf10-MI hearts 5 (MI-5d) and 21 (MI-21d) days after injury (Figure 4A). Immunofluorescence analysis of the proliferative capacities using Ki67 (Figure 4B-D and Supplemental Figure 4A), PH3 (Supplemental Figure 4B-C) and Aurora kinase B (AURKB, Figure 4E) revealed that upregulated *Fgf10* levels post-MI significantly enhances cardiomyocyte renewal in both IA and BZ. Interestingly, while *Fgf10* upregulation post-MI enhances cardiomyocyte renewal, it has no impact or even reduces proliferation of non-myocytes (Supplemental Figure 4D-E). This observed increase in cardiomyocyte cell cycle is specifically due to *Fgf10* upregulation since no change in the level of $Ki67^{+}$- or $PH3^{+}$-cardiomyocytes could be detected in DOX-*Rosa26-RTTA* compared to CTRL-*R26R-RTTA/Tet(O)-Fgf10* treated MI hearts (Supplemental Figure 4F-H). Analysis of cardiomyocyte cross-sectional area frequency within the injured ventricle revealed a significant upregulation of small cardiomyocytes in the BZ and IA of DOX- compared to CTRL-treated *R26R-RTTA/Tet(O)-Fgf10*-MI hearts (Figure 4F). This observation is consistent with the presence of newly formed cardiomyocytes following upregulation of FGF10 post-MI. Newly formed cardiomyocytes have been shown to arise from a rare proliferative subpopulation of mononucleated cardiomyocytes (17-19). We evaluated the impact of increased *Fgf10* levels on cardiomyocyte nucleation in pathological conditions using isolated cardiomyocytes from CTRL- and DOX-treated *R26R-RTTA/Tet(O)-Fgf10* hearts (Figure 4G-J). Our results demonstrated that after MI elevated FGF10 levels increased mononucleated cardiomyocyte numbers (Figure 4H-I). Immunofluorescence analysis of proliferative capacity using Ki67 revealed that FGF10 significantly enhances $Ki67^{+}$-mononucleated cardiomyocyte numbers post-MI (Figure 4J). Similar results were observed in normal conditions (Supplemental Figure 5A-D). To a lesser extent, FGF10 also increases $Ki67^{+}$-binucleated cardiomyocyte numbers (Supplemental Figure 5E). Finally, lineage tracing analysis using *αMHC-MerCreMer/R26R-tdT-RTTA/Tet(O)-Fgf10* mice confirmed the hypothesis that

the newly formed cardiomyocytes derived from pre-existing cardiomyocytes (Supplemental Figure 5A and F; 8159 counted cardiomyocytes, 100% $MF20^{+}Tomato^{+}$, n=9).

Myocardial infarction results in massive cardiomyocyte necrosis that leads to the release of myocardial biochemical markers, including Troponin T and I, in circulating blood (20). To address whether *Fgf10* upregulation post-MI affects cardiomyocyte necrosis, serum contents of cardiac troponin T (cTnT) and I (cTnI) were determined in CTRL- and DOX-MI mice (Supplemental Figure 6A). Our results revealed that both cTnT (Supplemental Figure 6B) and cTnI (Supplemental Figure 6C) serum levels were significantly reduced in DOX- compare to CTRL-treated MI mice suggesting that, in addition to promoting cardiomyocyte renewal, FGF10 prevents cardiomyocyte necrosis post-MI.

We then investigated the impact of *Fgf10* upregulation post-MI on cardiac fibrosis. Histological analysis using Sirius red staining and qRT-PCR analysis were performed. Decreased fibrosis was observed in DOX-treated *R26R-RTTA/Tet(O)-Fgf10*-MI hearts 21 days post-MI, compared to CTRL-treated *R26R-RTTA/Tet(O)-Fgf10*-MI hearts (Figure 4K-L). This was accompanied by downregulated collagen gene expression (Figure 4M). Finally, *in vitro* experiments using human cardiac fibroblasts demonstrated that FGF10 is able to significantly reduce TGF-β1-induced cardiac fibroblast activation into α-SMA (*Acta2*)-expressing myofibroblasts (Figure 4N), suggesting that FGF10 may play an upstream role in preventing fibrosis post-MI.

3.6 Molecular mechanisms underlying FGF10-induced cardiac regeneration and repair

To uncover the molecular mechanisms by which FGF10 promotes cardiac regeneration and repair following MI, genome wide transcriptomic analysis was performed by RNA-seq on IA from CTRL- and DOX-treated *Rosa26-RTTA/Tet(O)-Fgf10* 21 days post-injury (Figure 5).

Unsupervised clustering of the normalized expression values of the differentially expressed genes (DEG) strictly segregates DOX- from CTRL-treated *Rosa26-RTTA/Tet(O)-Fgf10* IA (Figure 5A). Among the 2016 DEG ($Log_2FC>0.5$; adjusted p-value<0.05), 831 were downregulated in DOX-*Rosa26-RTTA/Tet(O)-Fgf10*, and expression of 1185 genes was increased compared with CTRL-*Rosa26-RTTA/Tet(O)-Fgf10* (Figure 5B, Supplemental Table 1). As an internal control, we detected significant upregulation of *Fgf10* transcripts ($Log_2FC=5.4$, adjusted p-value=$6x10^{-7}$). Consistent with the activation of cardiac regenerative and repair processes, gene ontology enrichment analysis (Figure 5C) identified categories including heart process, developmental process, mitochondria, extracellular matrix and immune process. Myocardial infarction is associated with an early inflammatory response, which is a prerequisite for healing and scar formation (21). Since our RNAseq was performed 21 days post-MI, we thus evaluated a potential role for FGF10 in modulating myocardial levels of inflammatory cytokines and immune cell recruitment 5 days post-myocardial infarction. Myocardial expression analysis of key inflammatory cytokines and immune cell markers (monocytes and macrophages) was performed in CTRL- and DOX-treated *R26R-RTTA/Tet(O)-Fgf10*-MI hearts (Supplemental Figure 7A-C) and in WT- and *Fgf10*$^{+/-}$-MI hearts (Supplemental Figure 7D-F), nevertheless, no change in selected marker expression was detected. In addition to significant downregulation of genes involved in extracellular matrix remodeling, cardiac fibroblast markers including *Ddr2* and *Pdgfrα* display reduced expression (Figure 5E), consistent with reduced fibrosis in DOX- versus CTRL-treated *Rosa26-RTTA/Tet(O)-Fgf10* hearts post-MI (Figure 4K-M) and our experiments using human cardiac fibroblast cultures suggesting that FGF10 may play an upstream role in preventing fibrosis post-MI (Figure 4N).

KEGG pathway annotation analysis (Figure 5D) revealed critical signaling pathways overrepresented among selected DEG, including known downstream FGF10 signaling

cascades such as the MAPK, PI3K and FOXO pathways. Consistent with the impact of FGF10 on the activation of cardiomyocyte cell cycle reentry, multiple genes related to cell cycle modulation, including downregulated expression of a gene that negatively regulates cardiomyocyte cell cycle, *Meis1* (18, 22), were identified (Figure 5E). Metabolic pathways were also identified as overrepresented. FGF10 is known to potentiate, through the activation of the PI3K/AKT/mTOR pathway, HIF1α translation (23) which expression stabilization favors glycolytic metabolism (24). We found that increased *Fgf10* levels post-MI activate the PI3K pathway, including transcriptional upregulation of the mTOR gene, and significantly enhance HIF1α downstream target expression including glycolysis-related genes (Figure 5E). Our data thus demonstrate that *Fgf10* upregulation post-MI favors a strong metabolic switch towards glycolysis. As described in other tissues (24), the observed upregulation of the AMPK/fatty acid signaling cascade is consistent with the completion of the regenerative process ensuring re-differentiation of newly formed contractile cardiomyocytes. The Hippo pathway has been recently described to be a critical determinant for promoting adult cardiomyocyte cell cycle reentry (25). Our data revealed that enhanced *Fgf10* levels post-MI leads to the transcriptional activation of multiple key components of the Hippo pathway, including *Park2,* which has recently been shown to play an essential role in Hippo-induced heart repair and regeneration (26) (Figure 5E).

To confirm the crucial role of FGF10 in promoting the activation of signaling and cellular events required to promote cardiomyocyte cell cycle reentry, we evaluated the impact of decreased *Fgf10* dosage on the expression of genes encoding key glycolytic enzymes (*Pdk2* and *Eno3*), the transcription factor *Meis1* and the Hippo pathway member *Park2*, 21 days after myocardial infarction. Our results demonstrate that, compared to WT-MI hearts, *Fgf10*$^{+/-}$-MI

hearts display significantly reduced *Pdk2* and *Eno3* and *Park2* expression levels, whereas *Meis1* expression is enhanced (Supplemental Figure 8).

Together these results suggest that FGF10 promotes cardiac regeneration by modulating major regenerative pathways including the regulation of *Meis1* expression levels, the Hippo signaling pathway and a pro-glycolytic metabolic switch.

3.7 In failing human hearts, elevated *FGF10* expression correlates with high levels of cardiomyocyte proliferation and reduced cardiac fibrosis

We then investigated *FGF10* expression levels in failing explanted human heart samples (Supplemental Table 2). Transcript levels were quantified by qRT-PCR in different microdissected regions of explanted hearts. Our results revealed elevated *FGF10* levels in the injured ventricles compared to right ventricular *FGF10* levels. Indeed 4 out of 7 hearts displayed increased *FGF10* expression in the BZ and 5 out of 7 hearts displayed enhanced *FGF10* levels in the IA (Supplemental Figure 9A). We then evaluated whether human ventricular *FGF10* levels may influence cardiomyocyte renewal. Immunofluorescence experiments using Ki67 revealed that elevated *FGF10* levels significantly correlate with enhanced $Ki67^{+}$ cardiomyocyte numbers in the BZ (Figure 6A-B) and the IA (Supplemental Figure 9B-C). In the BZ, cardiomyocyte cross-sectional area measurement using WGA staining revealed that, except for heart sample B, elevated *FGF10* levels correlate with decreased cardiomyocyte cell size (Figure 6E and Supplemental Figure 9D-E). In addition, the analysis of cardiomyocyte size frequency Supplemental Figure 9F) demonstrated that elevated *FGF10* levels correlate with a high frequency of small cardiomyocytes (<600µm², Figure 6C) and with a low frequency of large cardiomyocytes (>800µm², Supplemental Figure 9G), suggesting that, consistent with our results in mice, higher *FGF10* levels in human hearts favors cardiomyocyte

renewal. Despite low *FGF10* expression levels in the BZ of patient B, a high frequency of small cardiomyocytes are observed in that area. This unexpected result may be explained by the high level of *FGF10* expression in the IA that may influence cardiomyocyte status in the adjacent BZ. Finally, to determine whether human myocardial *FGF10* levels influence cardiac fibrosis, histological analysis using Sirius red staining was performed and fibrosis was quantified. Our results demonstrated that elevated *FGF10* levels strongly correlate with reduced fibrosis in the IA (Figure 6D and F) and the BZ (Supplemental Figure 9H-I). These results obtained in human heart samples reinforce the conclusions of our mouse experiments and support the relevance for FGF10 in promoting cardiomyocyte renewal and preventing fibrosis.

4. DISCUSSION

In this study, we demonstrated that *Fgf10* expression post-MI promotes cardiac regeneration and repair through two cellular mechanisms: elevating cardiomyocyte renewal and limiting fibrosis. Our results suggest that FGF10 activates major regenerative pathways including the regulation of *Meis1* expression levels, the Hippo signaling pathway and a pro-glycolytic metabolic switch as well as playing a direct role in preventing cardiac myofibroblast activation. Moreover, elevated *FGF10* levels in failing explanted human heart samples strongly correlate with enhanced cardiomyocyte proliferation and reduced fibrosis. Together our study highlights the pro-regenerative capacities of FGF10 and supports FGF10 as a clinically relevant target for heart regeneration in man.

After birth, the vast majority of cardiomyocytes undergo maturation leading to multinucleation and metabolic switch toward oxidative phosphorylation (27, 28). Nevertheless, a rare population of resident adult mononucleated cardiomyocytes, generally smaller than binucleated cardiomyocytes, has been described to participate to cardiomyocyte renewal in normal aging (17, 19, 22, 29). We demonstrated that FGF10 enhances adult mononucleated cardiomyocyte numbers by promoting cell division of pre-existing adult mononucleated cardiomyocytes. However, since cytokinesis of binucleated cardiomyocytes is also possible (14), we cannot exclude that FGF10 may also promote binucleated cardiomyocyte cell division.

Cardiomyocyte metabolic reprogramming toward glycolysis, has been recently reported to be required for cardiac regeneration (30). Our data indicate that, through the activation of the mTOR/HIF1α pathway activation, FGF10 post-MI favors a glycolytic metabolic switch.

FGF-

dependent control of c-MYC expression that, in turn, regulates expression of glycolytic enzymes may also participate in the glycolytic metabolic switch (31).

Our results suggest that signaling events downstream of FGF10 may negatively regulate *Meis1*, allowing the removal of a cell cycle block leading to cardiomyocyte cell cycle reentry and cardiac regeneration. The transcription factor MEIS1 participates in postnatal cardiomyocyte cell cycle exit through the activation of cyclin-dependent kinase inhibitor expression and *Meis1* deletion in cardiomyocytes is sufficient to promote cardiomyocyte mitosis in the adult heart (22). Interestingly, the rare proliferative adult cardiomyocyte population is highly hypoxic (Hif1α-responsive) and displays decreased *Meis* family member gene expression (18).

The release of the Hippo block operating in mature cardiomyocytes seems to be a crucial checkpoint to enable cardiomyocytes to reenter the cell cycle and the modulation of Hippo pathway components critically participates in cardiac regeneration (25). Our study demonstrated significantly upregulated levels of the Hippo pathway downstream target *Park2* in *Fgf10*-overexpressing hearts. The ubiquitin ligase Parkin, encoded by the *Park2* gene, plays an essential role in normal postnatal cardiac mitochondrial and metabolic maturation by promoting mitophagy (32). *Park2* was also reported to play a critical role in the adaptive response after MI by promoting clearance of damaged mitochondria via autophagy (33). Recently, Leach *et al.*, revealed that *Park2* is essential for the Hippo-induced heart regeneration (26). In our study, *Park2* may thus also participate to the metabolic switch in response to forced *Fgf10* expression.

Decreased cardiomyocyte cell size has been shown to be an indicator of enhanced cardiomyocyte proliferation (17, 19, 22, 29). Our results demonstrating that FGF10 significantly increases the number of small cardiomyocyte in the injured ventricle strongly

supports FGF10-induced cardiomyocyte renewal. Cardiomyocyte cell size is nevertheless controlled by a balance between atrophic and hypertrophic signaling (34). Here, a role of FGF10 on the modulation of atrophic gene expression cannot be excluded. Indeed, among diverse genes described to regulate cardiac atrophy, we identified that FGF10 overexpression 21 days post-MI significantly upregulates *Murf1* transcript levels ($Log_2FC=2.7$, adjusted p-value=0.003).

In addition to promoting cardiomyocyte renewal, our data suggest that FGF10 exposure significantly decreases cardiac myofibroblast activation. Of particular interest, *Fgf10*-overexpression post-MI results in the significant downregulation of *Smoc1* and *Smoc2,* silencing of which has been recently shown to be required to prevent myofibroblast transformation (35, 36). Here, we cannot exclude a role for FGF10 in epicardial priming required for neovascularization (37) and the secretion of pro-regenerative signals in pathological conditions (38). Furthermore, FGF10 anti-inflammatory properties (39, 40) may potentially participate in the regenerative process induced by FGF10 treatment.

Alternatively, or in addition, the ability of FGF10 to promote functional cardiomyocyte differentiation during ESC/iPSC differentiation (41) and cardiac reprogramming (42), may also participate in the observed FGF10-induced cardioprotective effect.

In addition to ischemic-related pathologies, the therapeutic effect of FGF10 has been extensively studied in wound healing, venous ulcers, mucositis, or ulcerative colitis, leading to early human clinical studies clearly demonstrating FGF10 clinical safety and thus supporting its utilization in clinics (43, 44). The fact that in human terminal heart failure, elevated myocardial *FGF10* levels associate with enhanced cardiomyocyte proliferative capacities and reduced fibrosis reinforces our results obtained in mice. In contrast to mouse models, few experiments have addressed the capacity of human cardiomyocytes to respond to

536 regenerative signals (45, 46). Our results identify FGF10 as a potential regulator of
537 cardiomyocyte cell cycle and fibrosis in the adult human heart.
538 Together, our results indicate that FGF10 preserves cardiac remodeling and performance of
539 the injured heart, strongly supporting FGF10 as a clinical relevant target to promote cardiac
540 regeneration and repair in human patients.
541

DATA AVAILABILITY

The data underlying this article are available in the article and in its online supplementary material.

FUNDING

This work was supported by the Agence Nationale de la Recherche grant ANR-14-CE12-12-02, the Fédération Française de Cardiologie, and AFM-Téléthon grant no. 20777 awarded to FR and an AFM-Téléthon post-doctoral fellow awarded to FH.

ACKNOWLEDGEMENTS

We thank Valerie Delague, David Salgado and Laurent Argiro from the Genomics and Bioinformatics Platform (GBiM) from the U 1251/Marseille Medical Genetics for supervising and performing, respectively, the RNAseq experiments. We thank Regis Guieu (Laboratory of Biochemistry, Timone Hospital) for advice on biochemical analysis. We thank Patrick Lechêne (Inserm UMR-S 1180) for statistical advice. We are grateful to Rodolphe Fischmeister (Inserm UMR-S 1180) for his comments and advice on the manuscript.

CONFLICT OF INTEREST

The authors have declared that no conflict of interest exists.

REFERENCES

1. Benjamin EJ, Virani SS, Callaway CW, Chamberlain AM, Chang AR, Cheng S, Chiuve SE, Cushman M, Delling FN, Deo R, de Ferranti SD, Ferguson JF, Fornage M, Gillespie C, Isasi CR, Jimenez MC, Jordan LC, Judd SE, Lackland D, Lichtman JH, Lisabeth L, Liu S, Longenecker CT, Lutsey PL, Mackey JS, Matchar DB, Matsushita K, Mussolino ME, Nasir K, O'Flaherty M, Palaniappan LP, Pandey A, Pandey DK, Reeves MJ, Ritchey MD, Rodriguez CJ, Roth GA, Rosamond WD, Sampson UKA, Satou GM, Shah SH, Spartano NL, Tirschwell DL, Tsao CW, Voeks JH, Willey JZ, Wilkins JT, Wu JH, Alger HM, Wong SS, Muntner P, American Heart Association Council on E, Prevention Statistics C, and Stroke Statistics S. Heart Disease and Stroke Statistics-2018 Update: A Report From the American Heart Association. *Circulation.* 2018;137(12):e67-e492.
2. Bergmann O, Bhardwaj RD, Bernard S, Zdunek S, Barnabe-Heider F, Walsh S, Zupicich J, Alkass K, Buchholz BA, Druid H, Jovinge S, and Frisen J. Evidence for cardiomyocyte renewal in humans. *Science.* 2009;324(5923):98-102.
3. Eschenhagen T, Bolli R, Braun T, Field LJ, Fleischmann BK, Frisen J, Giacca M, Hare JM, Houser S, Lee RT, Marban E, Martin JF, Molkentin JD, Murry CE, Riley PR, Ruiz-Lozano P, Sadek HA, Sussman MA, and Hill JA. Cardiomyocyte Regeneration: A Consensus Statement. *Circulation.* 2017;136(7):680-6.
4. Tzahor E, and Poss KD. Cardiac regeneration strategies: Staying young at heart. *Science.* 2017;356(6342):1035-9.
5. Payan SM, Hubert F, and Rochais F. Cardiomyocyte proliferation, a target for cardiac regeneration. *Biochim Biophys Acta Mol Cell Res.* 2019.
6. Hortells L, Johansen AKZ, and Yutzey KE. Cardiac Fibroblasts and the Extracellular Matrix in Regenerative and Nonregenerative Hearts. *J Cardiovasc Dev Dis.* 2019;6(3).
7. Rochais F, Sturny R, Chao CM, Mesbah K, Bennett M, Mohun TJ, Bellusci S, and Kelly RG. FGF10 promotes regional foetal cardiomyocyte proliferation and adult cardiomyocyte cell-cycle re-entry. *Cardiovasc Res.* 2014;104(3):432-42.

8. Itoh N, Ohta H, Nakayama Y, and Konishi M. Roles of FGF Signals in Heart Development, Health, and Disease. *Front Cell Dev Biol.* 2016;4(110.
9. Hubert F, Payan SM, and Rochais F. FGF10 Signaling in Heart Development, Homeostasis, Disease and Repair. *Front Genet.* 2018;9(599.
10. Marguerie A, Bajolle F, Zaffran S, Brown NA, Dickson C, Buckingham ME, and Kelly RG. Congenital heart defects in Fgfr2-IIIb and Fgf10 mutant mice. *Cardiovasc Res.* 2006;71(1):50-60.
11. Takagawa J, Zhang Y, Wong ML, Sievers RE, Kapasi NK, Wang Y, Yeghiazarians Y, Lee RJ, Grossman W, and Springer ML. Myocardial infarct size measurement in the mouse chronic infarction model: comparison of area- and length-based approaches. *J Appl Physiol (1985).* 2007;102(6):2104-11.
12. Watanabe Y, Zaffran S, Kuroiwa A, Higuchi H, Ogura T, Harvey RP, Kelly RG, and Buckingham M. Fibroblast growth factor 10 gene regulation in the second heart field by Tbx1, Nkx2-5, and Islet1 reveals a genetic switch for down-regulation in the myocardium. *Proc Natl Acad Sci U S A.* 2012;109(45):18273-80.
13. Eulalio A, Mano M, Dal Ferro M, Zentilin L, Sinagra G, Zacchigna S, and Giacca M. Functional screening identifies miRNAs inducing cardiac regeneration. *Nature.* 2012;492(7429):376-81.
14. D'Uva G, Aharonov A, Lauriola M, Kain D, Yahalom-Ronen Y, Carvalho S, Weisinger K, Bassat E, Rajchman D, Yifa O, Lysenko M, Konfino T, Hegesh J, Brenner O, Neeman M, Yarden Y, Leor J, Sarig R, Harvey RP, and Tzahor E. ERBB2 triggers mammalian heart regeneration by promoting cardiomyocyte dedifferentiation and proliferation. *Nat Cell Biol.* 2015;17(5):627-38.
15. Jopling C, Sleep E, Raya M, Marti M, Raya A, and Izpisua Belmonte JC. Zebrafish heart regeneration occurs by cardiomyocyte dedifferentiation and proliferation. *Nature.* 2010;464(7288):606-9.
16. Zhang Y, Li S, Yuan L, Tian Y, Weidenfeld J, Yang J, Liu F, Chokas AL, and Morrisey EE. Foxp1 coordinates cardiomyocyte proliferation through both cell-autonomous and nonautonomous mechanisms. *Genes Dev.* 2010;24(16):1746-57.
17. Patterson M, Barske L, Van Handel B, Rau CD, Gan P, Sharma A, Parikh S, Denholtz M, Huang Y, Yamaguchi Y, Shen H, Allayee H, Crump JG, Force TI, Lien CL, Makita T, Lusis AJ, Kumar SR, and Sucov

617 HM. Frequency of mononuclear diploid cardiomyocytes underlies natural variation in heart
618 regeneration. *Nature genetics.* 2017;49(9):1346-53.
619 18. Kimura W, Xiao F, Canseco DC, Muralidhar S, Thet S, Zhang HM, Abderrahman Y, Chen R, Garcia JA,
620 Shelton JM, Richardson JA, Ashour AM, Asaithamby A, Liang H, Xing C, Lu Z, Zhang CC, and Sadek
621 HA. Hypoxia fate mapping identifies cycling cardiomyocytes in the adult heart. *Nature.*
622 2015;523(7559):226-30.
623 19. Bersell K, Arab S, Haring B, and Kuhn B. Neuregulin1/ErbB4 signaling induces cardiomyocyte
624 proliferation and repair of heart injury. *Cell.* 2009;138(2):257-70.
625 20. Park KC, Gaze DC, Collinson PO, and Marber MS. Cardiac troponins: from myocardial infarction to
626 chronic disease. *Cardiovasc Res.* 2017;113(14):1708-18.
627 21. Frangogiannis NG, Smith CW, and Entman ML. The inflammatory response in myocardial infarction.
628 *Cardiovasc Res.* 2002;53(1):31-47.
629 22. Mahmoud AI, Kocabas F, Muralidhar SA, Kimura W, Koura AS, Thet S, Porrello ER, and Sadek HA.
630 Meis1 regulates postnatal cardiomyocyte cell cycle arrest. *Nature.* 2013;497(7448):249-53.
631 23. Walker DJ, and Land SC. Regulation of vascular signalling by nuclear Sprouty2 in fetal lung epithelial
632 cells: Implications for co-ordinated airway and vascular branching in lung development. *Comp*
633 *Biochem Physiol B Biochem Mol Biol.* 2018;224(105-14.
634 24. Heber-Katz E. Oxygen, Metabolism, and Regeneration: Lessons from Mice. *Trends Mol Med.*
635 2017;23(11):1024-36.
636 25. Wang J, Liu S, Heallen T, and Martin JF. The Hippo pathway in the heart: pivotal roles in
637 development, disease, and regeneration. *Nat Rev Cardiol.* 2018;15(11):672-84.
638 26. Leach JP, Heallen T, Zhang M, Rahmani M, Morikawa Y, Hill MC, Segura A, Willerson JT, and Martin
639 JF. Hippo pathway deficiency reverses systolic heart failure after infarction. *Nature.*
640 2017;550(7675):260-4.
641 27. Soonpaa MH, Kim KK, Pajak L, Franklin M, and Field LJ. Cardiomyocyte DNA synthesis and
642 binucleation during murine development. *Am J Physiol.* 1996;271(5 Pt 2):H2183-9.

643 28. Piquereau J, and Ventura-Clapier R. Maturation of Cardiac Energy Metabolism During Perinatal
644 Development. *Front Physiol.* 2018;9(959.
645 29. Senyo SE, Steinhauser ML, Pizzimenti CL, Yang VK, Cai L, Wang M, Wu TD, Guerquin-Kern JL, Lechene
646 CP, and Lee RT. Mammalian heart renewal by pre-existing cardiomyocytes. *Nature.*
647 2013;493(7432):433-6.
648 30. Honkoop H, de Bakker DE, Aharonov A, Kruse F, Shakked A, Nguyen PD, de Heus C, Garric L, Muraro
649 MJ, Shoffner A, Tessadori F, Peterson JC, Noort W, Bertozzi A, Weidinger G, Posthuma G, Grun D,
650 van der Laarse WJ, Klumperman J, Jaspers RT, Poss KD, van Oudenaarden A, Tzahor E, and Bakkers
651 J. Single-cell analysis uncovers that metabolic reprogramming by ErbB2 signaling is essential for
652 cardiomyocyte proliferation in the regenerating heart. *Elife.* 2019;8(
653 31. Yu P, Wilhelm K, Dubrac A, Tung JK, Alves TC, Fang JS, Xie Y, Zhu J, Chen Z, De Smet F, Zhang J, Jin
654 SW, Sun L, Sun H, Kibbey RG, Hirschi KK, Hay N, Carmeliet P, Chittenden TW, Eichmann A, Potente
655 M, and Simons M. FGF-dependent metabolic control of vascular development. *Nature.*
656 2017;545(7653):224-8.
657 32. Gong G, Song M, Csordas G, Kelly DP, Matkovich SJ, and Dorn GW, 2nd. Parkin-mediated mitophagy
658 directs perinatal cardiac metabolic maturation in mice. *Science.* 2015;350(6265):aad2459.
659 33. Kubli DA, Zhang X, Lee Y, Hanna RA, Quinsay MN, Nguyen CK, Jimenez R, Petrosyan S, Murphy AN,
660 and Gustafsson AB. Parkin protein deficiency exacerbates cardiac injury and reduces survival
661 following myocardial infarction. *J Biol Chem.* 2013;288(2):915-26.
662 34. Razeghi P, and Taegtmeyer H. Hypertrophy and atrophy of the heart: the other side of remodeling.
663 *Ann N Y Acad Sci.* 2006;1080(110-9.
664 35. Gerarduzzi C, Kumar RK, Trivedi P, Ajay AK, Iyer A, Boswell S, Hutchinson JN, Waikar SS, and Vaidya
665 VS. Silencing SMOC2 ameliorates kidney fibrosis by inhibiting fibroblast to myofibroblast
666 transformation. *JCI Insight.* 2017;2(8).

667 36. Wang Y, and Wu X. SMOC1 silencing suppresses the angiotensin II-induced myocardial fibrosis of
668 mouse myocardial fibroblasts via affecting the BMP2/Smad pathway. *Oncol Lett.* 2018;16(3):2903-
669 10.
670 37. Vega-Hernandez M, Kovacs A, De Langhe S, and Ornitz DM. FGF10/FGFR2b signaling is essential for
671 cardiac fibroblast development and growth of the myocardium. *Development.* 2011;138(15):3331-
672 40.
673 38. Cao J, and Poss KD. The epicardium as a hub for heart regeneration. *Nat Rev Cardiol.*
674 2018;15(10):631-47.
675 39. Li YH, Fu HL, Tian ML, Wang YQ, Chen W, Cai LL, Zhou XH, and Yuan HB. Neuron-derived FGF10
676 ameliorates cerebral ischemia injury via inhibiting NF-kappaB-dependent neuroinflammation and
677 activating PI3K/Akt survival signaling pathway in mice. *Sci Rep.* 2016;6(19869.
678 40. Tan X, Zhu H, Tao Q, Guo L, Jiang T, Xu L, Yang R, Wei X, Wu J, Li X, and Zhang JS. FGF10 Protects
679 Against Renal Ischemia/Reperfusion Injury by Regulating Autophagy and Inflammatory Signaling.
680 *Front Genet.* 2018;9(556.
681 41. Chan SS, Li HJ, Hsueh YC, Lee DS, Chen JH, Hwang SM, Chen CY, Shih E, and Hsieh PC. Fibroblast
682 growth factor-10 promotes cardiomyocyte differentiation from embryonic and induced pluripotent
683 stem cells. *PLoS One.* 2010;5(12):e14414.
684 42. Yamakawa H, Muraoka N, Miyamoto K, Sadahiro T, Isomi M, Haginiwa S, Kojima H, Umei T, Akiyama
685 M, Kuishi Y, Kurokawa J, Furukawa T, Fukuda K, and Ieda M. Fibroblast Growth Factors and Vascular
686 Endothelial Growth Factor Promote Cardiac Reprogramming under Defined Conditions. *Stem Cell*
687 *Reports.* 2015;5(6):1128-42.
688 43. Beenken A, and Mohammadi M. The FGF family: biology, pathophysiology and therapy. *Nat Rev*
689 *Drug Discov.* 2009;8(3):235-53.
690 44. Plichta JK, and Radek KA. Sugar-coating wound repair: a review of FGF-10 and dermatan sulfate in
691 wound healing and their potential application in burn wounds. *J Burn Care Res.* 2012;33(3):299-
692 310.

693 45. Polizzotti BD, Ganapathy B, Walsh S, Choudhury S, Ammanamanchi N, Bennett DG, dos Remedios
694 CG, Haubner BJ, Penninger JM, and Kuhn B. Neuregulin stimulation of cardiomyocyte regeneration
695 in mice and human myocardium reveals a therapeutic window. *Sci Transl Med.*
696 2015;7(281):281ra45.
697 46. Canseco DC, Kimura W, Garg S, Mukherjee S, Bhattacharya S, Abdisalaam S, Das S, Asaithamby A,
698 Mammen PP, and Sadek HA. Human ventricular unloading induces cardiomyocyte proliferation. *J*
699 *Am Coll Cardiol.* 2015;65(9):892-900.

FIGURE LEGENDS

Figure 1: Decreased *Fgf10* dosage worsens cardiac function and remodeling following myocardial infarction. (A) Schematic of the experimental plan. WT and *Fgf10*$^{+/-}$ adult mice were subjected to myocardial infarction (MI) and analysis were performed 21 days after surgery. (**B**) Heart weight/body weight ratio. WT-MI, n=26; *Fgf10*$^{+/-}$-MI, n=24. (**C**) Heart weight/tibia length ratio. WT-MI, n=20; *Fgf10*$^{+/-}$-MI, n=23. (**D**) M-mode images of echocardiographic experiments (Scale bars, x: 0.1 s; y: 1 mm). (**E**) Ejection fraction. (**F**) Fractional shortening. (**G**) Left ventricular systolic volume. WT-SHAM, n=14; *Fgf10*$^{+/-}$-SHAM, n=7; WT-MI, n=8; *Fgf10*$^{+/-}$-MI, n=6 (**H**) qRT-PCR analysis, on left ventricular tissues, of *Nppa* (n=5/group), *Nppb* (n=6/group) and *Myh7* (n=5-6/group) expression. *, $p<0.05$; **, $0,001<p<0.01$; ***, $p<0.001$; Student's *t*-test.

Figure 2: Decreased *Fgf10* dosage impairs cardiomyocyte proliferation and worsens fibrosis following MI. (**A**) Schematic of the experimental plan. WT and *Fgf10*$^{+/-}$ adult mice were subjected to myocardial infarction (MI) and analysis were performed 5 and 21 days after surgery. (**B-D**) Immunofluorescence experiments were performed to evaluate in the border zone *in vivo* cardiomyocyte proliferation (MF20^{+}; yellow arrowheads) 5 days (**C**; MI-5d; WT, n=6; *Fgf10*$^{+/-}$, n=5) and 21 days (**D**; MI-21d; WT, n=5; *Fgf10*$^{+/-}$, n=6) post-MI using Ki67. (**E**) Immunofluorescence experiments using Aurora B marker were performed to evaluate *in vivo* cardiomyocyte proliferation (MF20^{+}; yellow arrowheads) 5 days post-MI (n=6 mice/group). Scale bars, 10 µm (**B**) and 5 µm (**E**). (**F**) Cardiomyocyte cross-sectional area frequency (MI-21d; WT, n=6; *Fgf10*$^{+/-}$, n=5; compared using Fisher statistical test). (**G-H**) Histological sirius red staining was performed 5 days post-MI (WT, n=6; *Fgf10*$^{+/-}$, n=5, Scale bar, 1000 µm). (**I**) qRT-

PCR analysis 5 days post-MI of *Col1A1* (WT, n=5; *Fgf10*$^{+/-}$, n=7) and *Col3A1* (WT, n=6; *Fgf10*$^{+/-}$, n=6) expression in the border zone. (**J-K**) Histological sirius red staining was performed 21 days post-MI (WT, n=5; *Fgf10*$^{+/-}$, n=5, Scale bar, 1000 µm). (**L**) qRT-PCR analysis 21 days post-MI of *Col1A1* (WT, n=7; *Fgf10*$^{+/-}$, n=5), *Col3A1* (WT, n=6; *Fgf10*$^{+/-}$, n=5) and *Col6A5* (WT, n=6; *Fgf10*$^{+/-}$, n=5) expression in the infarcted area. ns, non-significant; *, p<0.05; **, 0,001<p<0.01; ***, p<0.001; Student's *t*-test.

Figure 3: Upregulation of *Fgf10* levels post-MI preserves cardiac function and remodeling. **(A)** Schematic of the experimental plan. *R26R-RTTA/Tet(O)-Fgf10* mice were subjected to myocardial infarction (MI). One day after MI, mice were fed with normal (CTRL) or doxycycline supplemented food (DOX) required to induce *Fgf10* overexpression and analyzed 21 days later. (**B**) Heart weight/body weight ratio. MI-CTRL, n=18; MI-DOX, n=25. (**C**) Heart weight/tibia length ratio. MI-CTRL, n=16; MI-DOX, n=25. (**D**) M-mode images of echocardiographic experiments (Scale bars, x: 0.1 s; y: 1 mm). (**E**) Ejection fraction. (**F**) Fractional shortening. (**G**) Left ventricular systolic volume. SHAM-CTRL, n=7; SHAM-DOX, n=6; MI-CTRL, n=12; MI-DOX, n=14. (**H**) qRT-PCR analysis, on left ventricular tissues, of *Nppa* (MI-CTRL, n=6; MI-DOX, n=7), *Nppb* (MI-CTRL, n=7; MI-DOX, n=7) and *Myh7* (MI-CTRL, n=6; MI-DOX, n=7) expression. ns, non-significant; *, p<0.05; **, 0,001<p<0.01; ***, p<0.001; Student's *t*-test.

Figure 4: Upregulation of *Fgf10* levels post-MI promotes cardiomyocyte cell cycle reentry and prevents fibrosis. (**A**) Schematic of the experimental plan. *R26R-RTTA/Tet(O)-Fgf10* mice were subjected to myocardial infarction (MI). One day after MI, mice were fed with normal (CTRL) or doxycycline supplemented food (DOX) required to induce *Fgf10* overexpression and

analyzed 5 and 21 days later. (**B**-**E**) Immunofluorescence experiments were performed to evaluate, 5 (MI-5d) and 21 (MI-21d) days post-MI, in the border zone (BZ) and in the infarcted area (IA), cardiomyocyte ($MF20^+$; yellow arrowheads) proliferation using $Ki67^+$ (**C,** MI-5d; BZ CTRL n=5, BZ DOX n=5, IA CTRL n=5, IA DOX n=5 and **D,** MI-21d; BZ CTRL n=6, BZ DOX n=7, IA CTRL n=6, IA DOX n=6) and $AURKB^+$ (**E**, n=5/group). (**F**) Cardiomyocyte cross-sectional area (n=6-7 mice/group). Scale bars, B: 10 µm; E: 5 µm and F: 25 µm. (**G**) *R26R-RTTA/Tet(O)-Fgf10* mice were subjected to myocardial infarction (MI). One day after MI, mice were fed with normal (CTRL) or doxycycline (DOX) supplemented food for 5 days. (**H-J**) Cardiomyocytes were isolated and immunofluorescence experiments were performed to evaluate mononucleated cardiomyocyte numbers (**I**) and their proliferative capacities (**J)**; (n=5-6/group). (**K-L**) Fibrosis was investigated 21 days post-MI using histological sirius red staining. n=5/group. Scale bars, 1000 µm. (**M**) qRT-PCR analysis of *Col1A1* (n=6/group), *Col3A1* (n=6/group) and *Col6A5* (CTRL n=6 Dox n=7) expression in the infarcted area. (**N**) Human fibroblast cultures revealed that FGF10 prevents TGF-β1-induced fibroblast activation, (n=3/group). ns, non-significant; *, $p<0.05$; **, $0,001<p<0.01$; ***, $p<0,001$; Student's *t*-test.

Figure 5: RNA-seq analysis reveals FGF10-induced transcriptional regulation of major regenerative pathways. *R26R-RTTA/Tet(O)-Fgf10* mice were subjected to myocardial infarction (MI). One day after MI, mice were fed with normal (CTRL) or doxycycline (DOX) supplemented food required to induce *Fgf10* overexpression. 21 days post-MI, RNA-seq analysis was performed in the infarcted area. (**A**) Heatmap showing hierarchical clustering of DEG in biological replicates (n=4/group). (**B**) Volcano plot of DEG sorted according to fold change and significance (FDR adjusted p-value). DEG (FDR < 0.05, n=2016) are shown in red, and non-significant changes are shown in black. (**C**) Enrichment analysis of gene ontology

terms for differentially regulated genes. Upregulated and downregulated genes in MI-DOX vs MI-CTRL are represented in red and blue, respectively. (**D**) Circular plot of 42 DEG showing the relationship between expression changes (left semicircle perimeter) and KEGG pathways (right semicircle perimeter). Changes in expression are represented for each gene as Log_2FC. (**E**) qRT-PCR experiments showing the validation of major candidate genes (n=4-6/group).

Figure 6: Upregulation of *FGF10* in human failing hearts correlates with increased cardiomyocyte proliferation, reduced cardiomyocyte size and reduced fibrosis. Human explanted failing heart samples from right ventricle (RV), remote area (RA), border zone (BZ) and infarcted area (IA) were collected from 7 patients (A-G). (**A**) Cardiomyocyte proliferation in the BZ was evaluated using immunofluorescence experiments and the cell cycle marker Ki67. (**B**) Elevated *FGF10* levels correlate with enhanced cardiomyocyte proliferation in the BZ. (**C**) Cardiomyocyte cross-sectional area was measured in the BZ using the cell membrane marker WGA. Elevated *FGF10* levels correlate with high frequency of small cardiomyocyte (<600µm²). (**D**) Cardiac fibrosis in the IA was assessed using histological Sirius red staining. Elevated FGF10 levels correlate with reduced fibrosis in the IA. (**E**) Representative pictures of WGA staining, according to patient-corresponding *FGF10* levels depicted in Supplemental Figure 8A, have been classified from low to high expression as represented by the above grey triangle. Scale bar 10 µm. (**E-F**) Representative pictures of Sirius red staining, according to patient-corresponding *FGF10* levels depicted in Supplemental Figure 8A, have been classified from low to high expression as represented by the above grey triangle. Scale bars 100 µm. Statistical significance (p) was determined using Student's *t*-distribution.

FIGURE 1

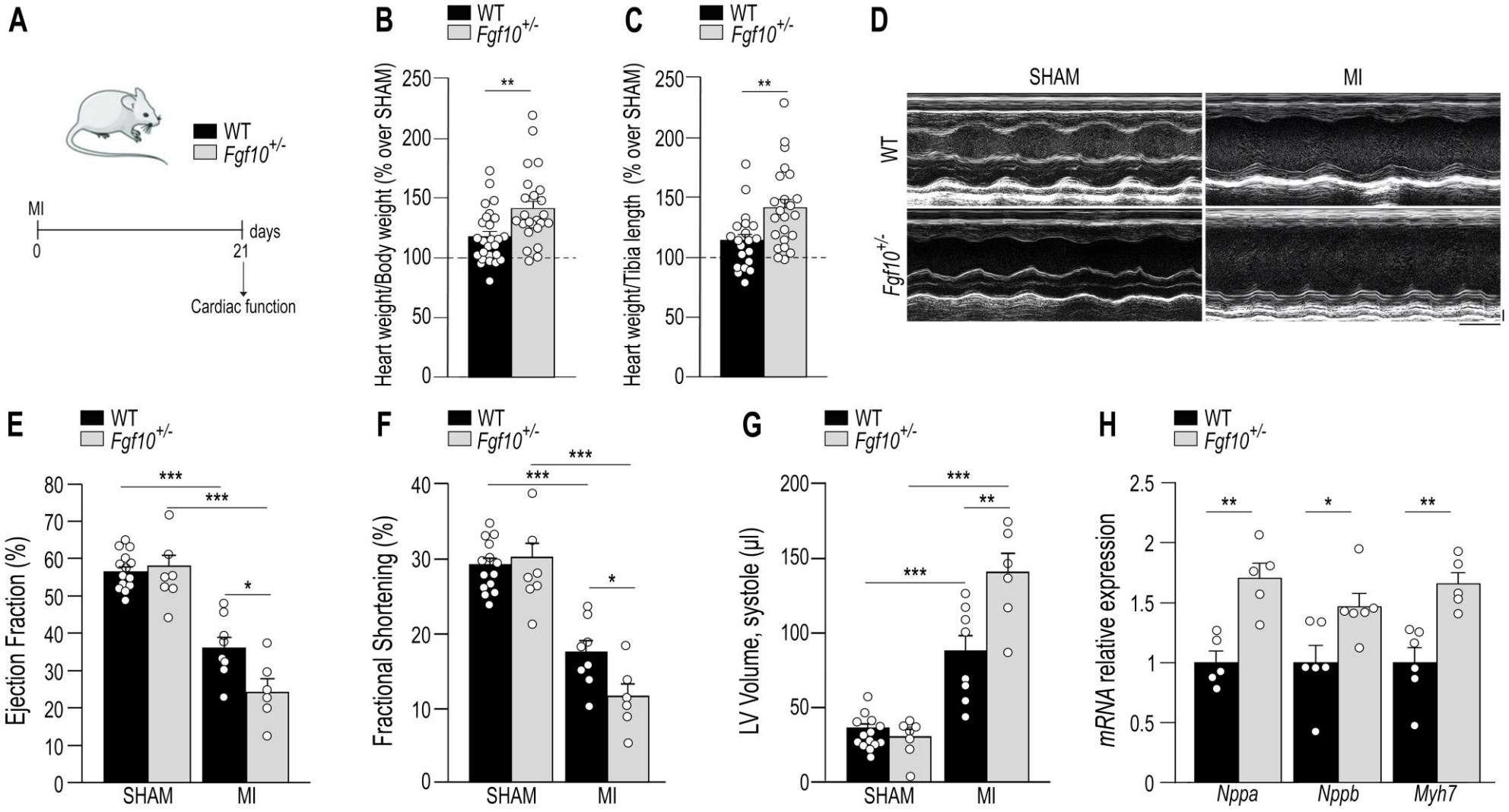
A
WT
Fgf10+/-
MI
0
21
days
Cardiac function
B
WT
Fgf10+/-
Heart weight/Body weight (% over SHAM)
C
WT
Fgf10+/-
Heart weight/Tibia length (% over SHAM)
D
SHAM
MI
WT
Fgf10+/-
E
WT
Fgf10+/-
Ejection Fraction (%)
SHAM
MI
F
WT
Fgf10+/-
Fractional Shortening (%)
SHAM
MI
G
WT
Fgf10+/-
LV Volume, systole (µl)
SHAM
MI
H
WT
Fgf10+/-
mRNA relative expression
Nppa
Nppb
Myh7

FIGURE 2

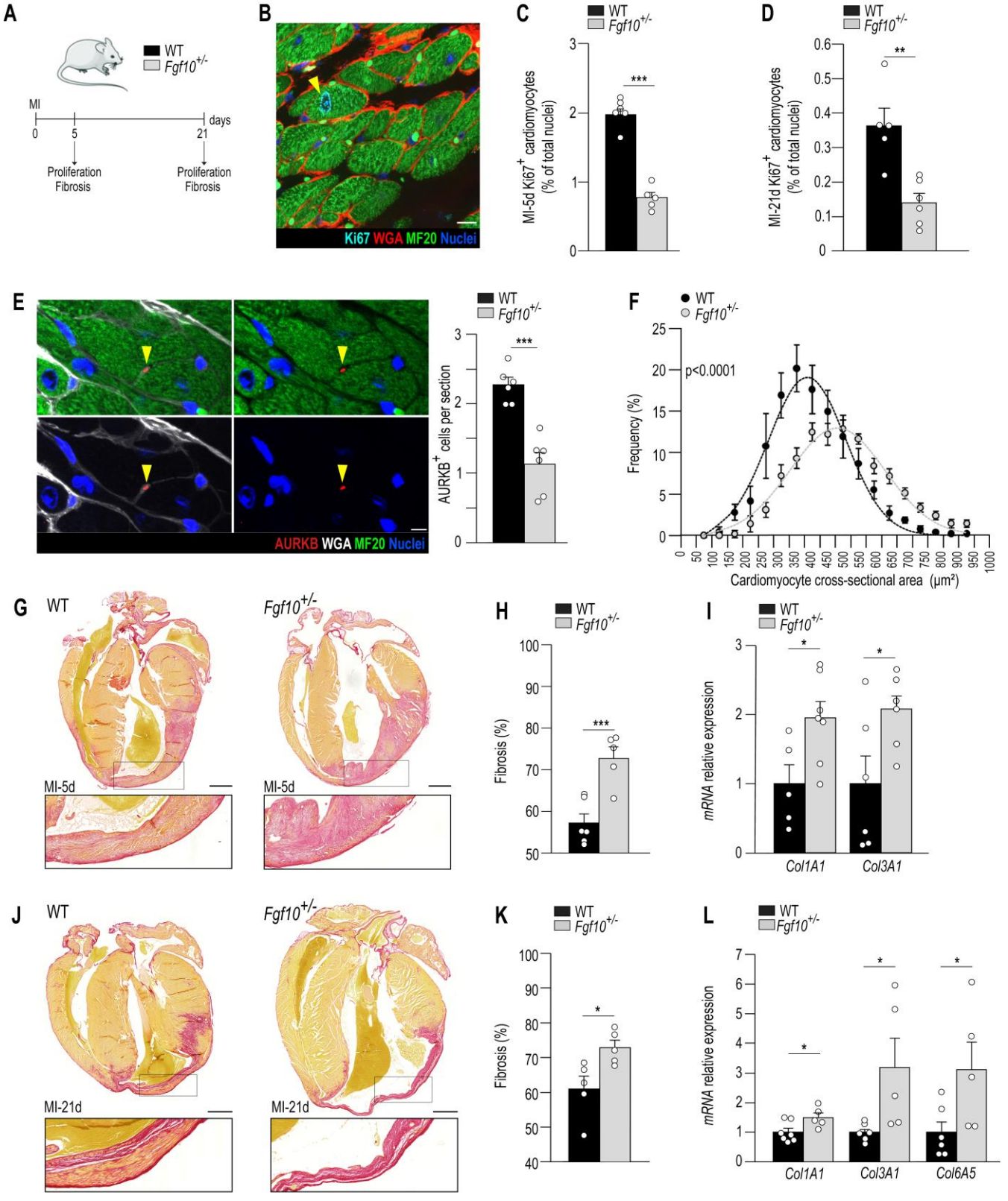
A
WT
Fgf10+/-
MI
0
5
21
days
Proliferation
Fibrosis
Proliferation
Fibrosis
B
Ki67 WGA MF20 Nuclei
C
WT
Fgf10+/-
MI-5d Ki67+ cardiomyocytes (% of total nuclei)
***
D
WT
Fgf10+/-
MI-21d Ki67+ cardiomyocytes (% of total nuclei)
**
E
AURKB WGA MF20 Nuclei
WT
Fgf10+/-
AURKB+ cells per section
***
F
WT
Fgf10+/-
p<0.0001
Frequency (%)
Cardiomyocyte cross-sectional area (µm²)
G
WT
Fgf10+/-
MI-5d
MI-5d
H
WT
Fgf10+/-
Fibrosis (%)
***
I
WT
Fgf10+/-
mRNA relative expression
*
*
Col1A1
Col3A1
J
WT
Fgf10+/-
MI-21d
MI-21d
K
WT
Fgf10+/-
Fibrosis (%)
*
L
WT
Fgf10+/-
mRNA relative expression
*
*
*
Col1A1
Col3A1
Col6A5

FIGURE 3

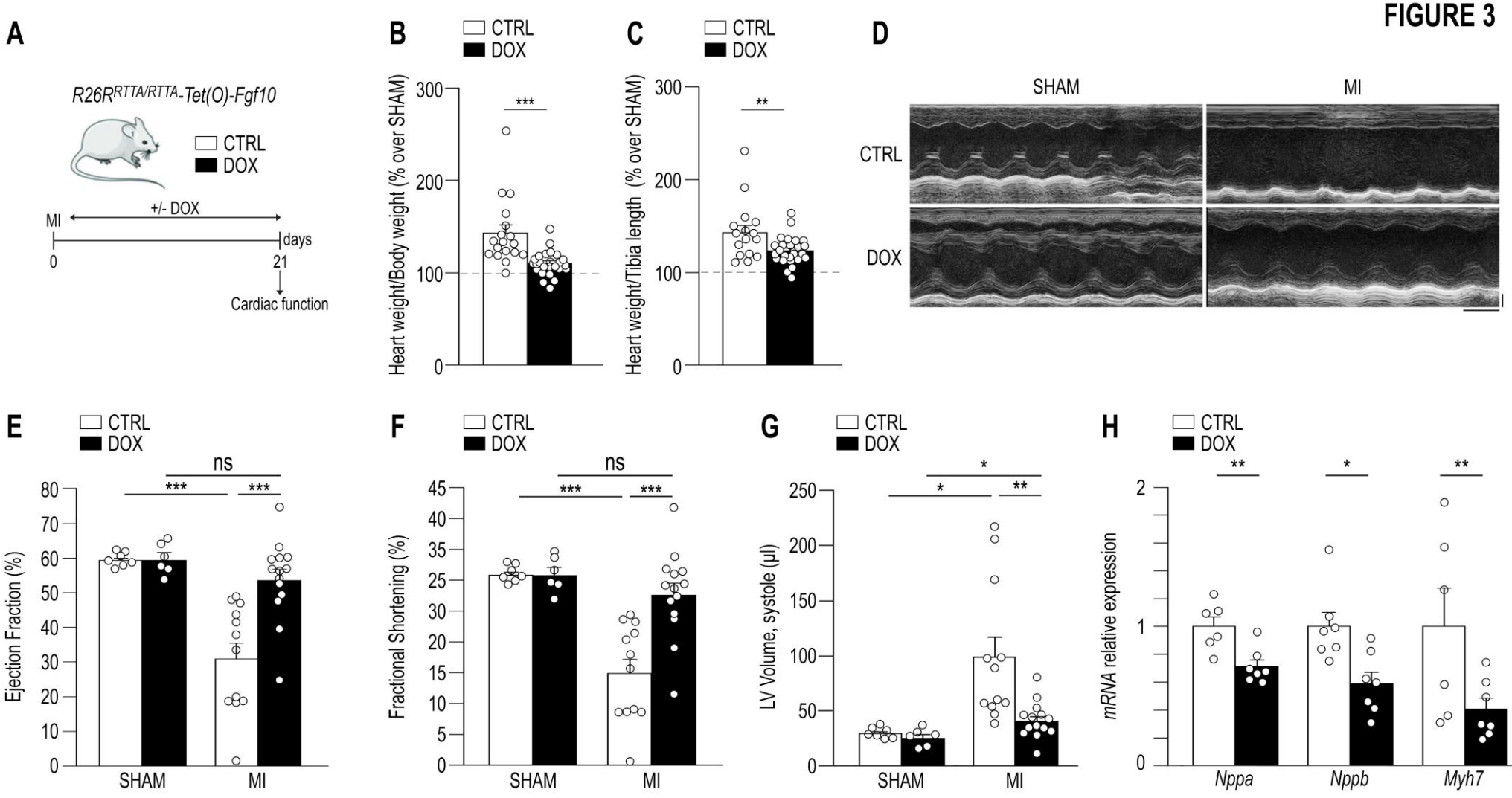
A
R26R^RTTA/RTTA-Tet(O)-Fgf10
CTRL
DOX
MI
+/- DOX
days
0
21
Cardiac function
B
CTRL
DOX
Heart weight/Body weight (% over SHAM)
300
200
100
0
***
C
CTRL
DOX
Heart weight/Tibia length (% over SHAM)
300
200
100
0
**
D
SHAM
MI
CTRL
DOX
E
CTRL
DOX
Ejection Fraction (%)
80
70
60
50
40
30
20
10
0
ns
***
***
SHAM
MI
F
CTRL
DOX
Fractional Shortening (%)
45
40
35
30
25
20
15
10
5
0
ns
***
***
SHAM
MI
G
CTRL
DOX
LV Volume, systole (µl)
250
200
150
100
50
0
*
*
**
SHAM
MI
H
CTRL
DOX
mRNA relative expression
2
1
0
**
*
**
Nppa
Nppb
Myh7

FIGURE 4

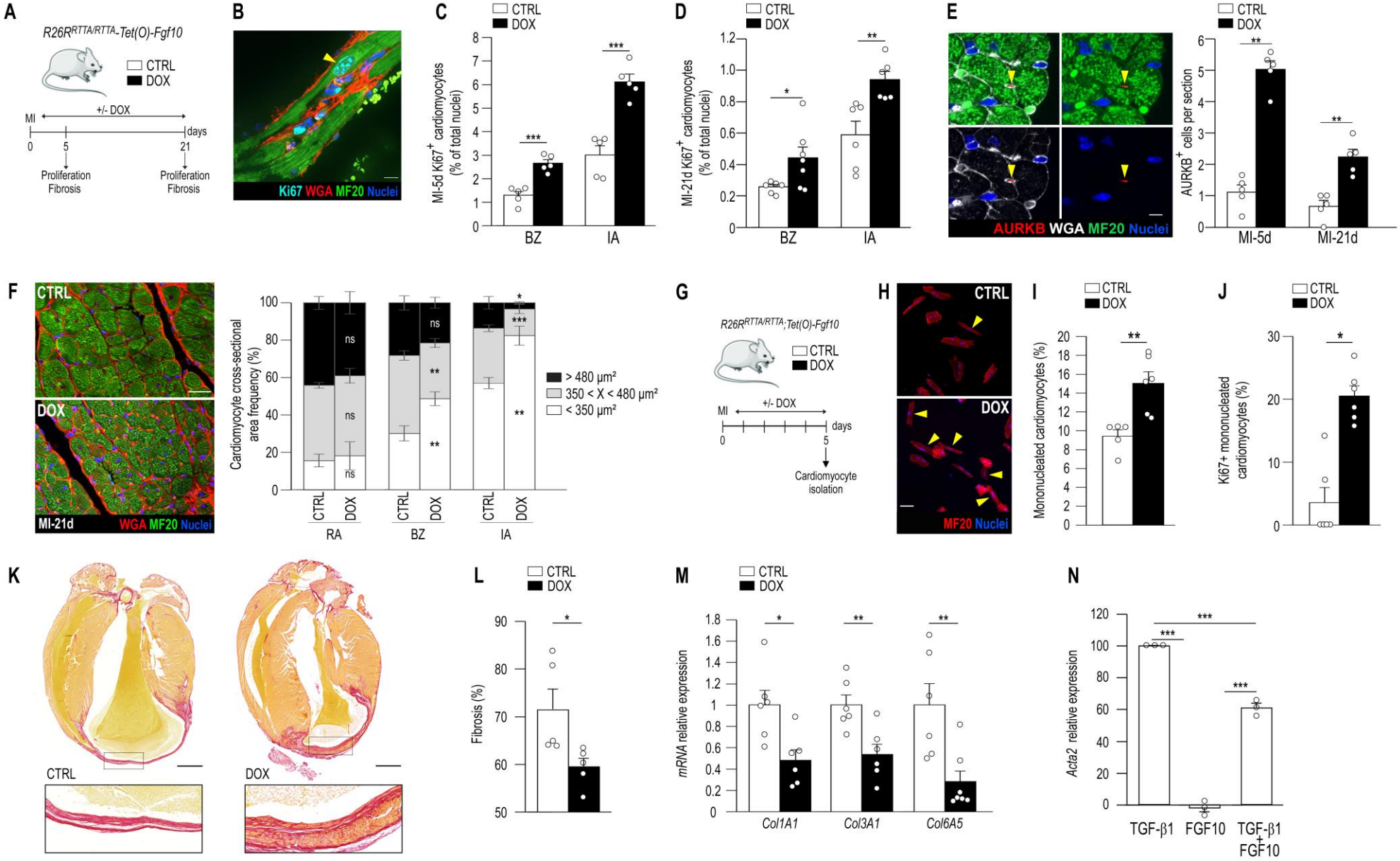
A
R26R^RTTA/RTTA-Tet(O)-Fgf10
CTRL
DOX
MI
+/- DOX
0
5
21
days
Proliferation
Fibrosis
Proliferation
Fibrosis
B
Ki67 WGA MF20 Nuclei
C
CTRL
DOX
MI-5d Ki67+ cardiomyocytes (% of total nuclei)
BZ
IA
D
CTRL
DOX
MI-21d Ki67+ cardiomyocytes (% of total nuclei)
BZ
IA
E
AURKB WGA MF20 Nuclei
CTRL
DOX
AURKB+ cells per section
MI-5d
MI-21d
F
CTRL
DOX
MI-21d
WGA MF20 Nuclei
Cardiomyocyte cross-sectional area frequency (%)
> 480 µm²
350 < X < 480 µm²
< 350 µm²
ns
RA
BZ
IA
G
R26R^RTTA/RTTA;Tet(O)-Fgf10
CTRL
DOX
MI
+/- DOX
0
5
days
Cardiomyocyte isolation
H
CTRL
DOX
MF20 Nuclei
I
CTRL
DOX
Mononucleated cardiomyocytes (%)
J
CTRL
DOX
Ki67+ mononucleated cardiomyocytes (%)
K
CTRL
DOX
L
CTRL
DOX
Fibrosis (%)
M
CTRL
DOX
mRNA relative expression
Col1A1
Col3A1
Col6A5
N
Acta2 relative expression
TGF-β1
FGF10
TGF-β1 + FGF10

FIGURE 5

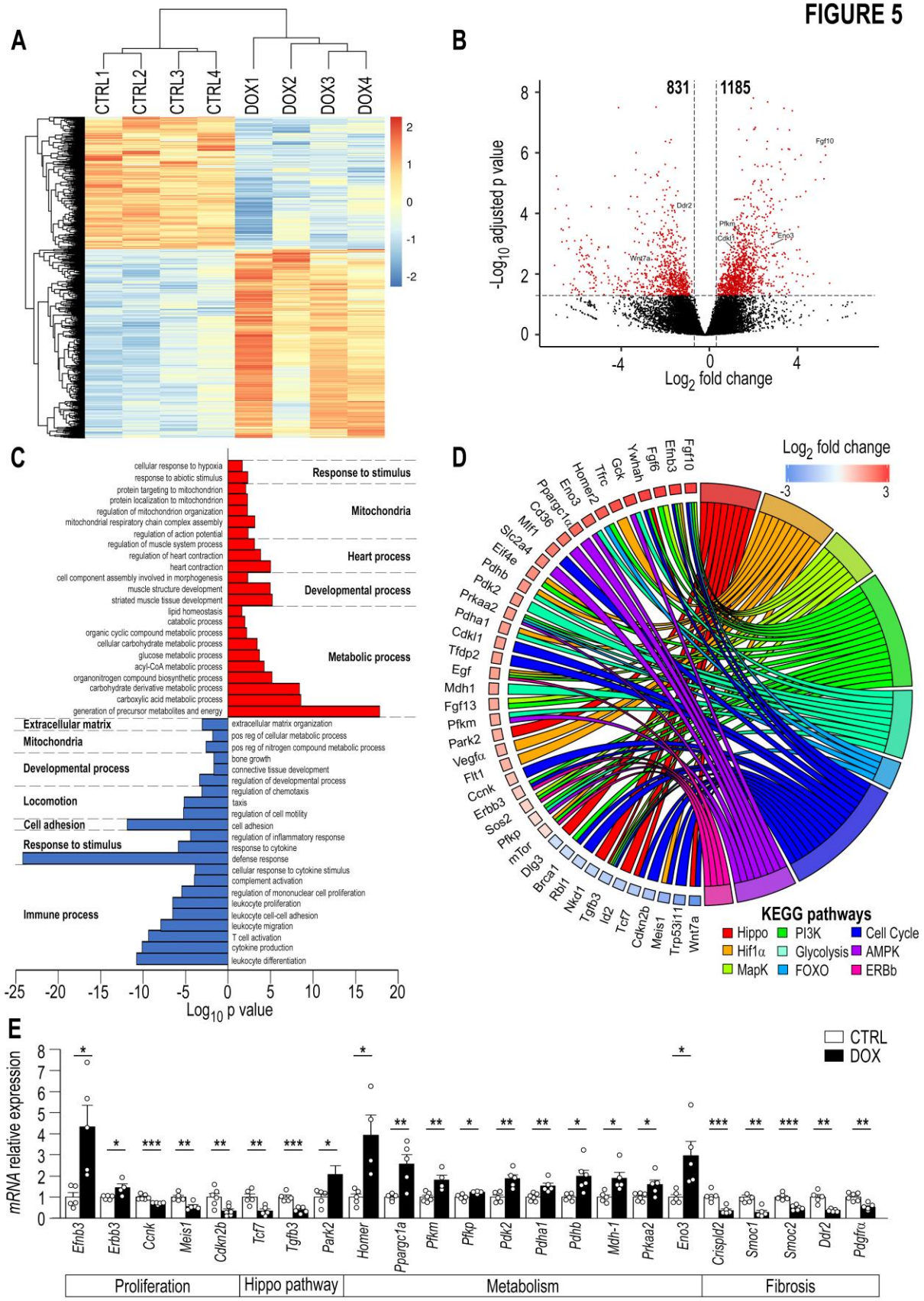
A
CTRL1
CTRL2
CTRL3
CTRL4
DOX1
DOX2
DOX3
DOX4
B
831
1185
-Log10 adjusted p value
Log2 fold change
Fgf10
Ddr2
Pfkm
Cdkl1
Eno3
Wnt7a
C
Response to stimulus
Mitochondria
Heart process
Developmental process
Metabolic process
Extracellular matrix
Locomotion
Cell adhesion
Immune process
Log10 p value
D
Log2 fold change
KEGG pathways
Hippo
PI3K
Cell Cycle
Hif1α
Glycolysis
AMPK
MapK
FOXO
ERBb
E
CTRL
DOX
mRNA relative expression
Efnb3
Erbb3
Ccnk
Meis1
Cdkn2b
Tcf7
Tgfb3
Park2
Homer
Ppargc1a
Pfkm
Pfkp
Pdk2
Pdha1
Pdhb
Mdh-1
Prkaa2
Eno3
Crispld2
Smoc1
Smoc2
Ddr2
Pdgfrα
Proliferation
Hippo pathway
Metabolism
Fibrosis

FIGURE 6

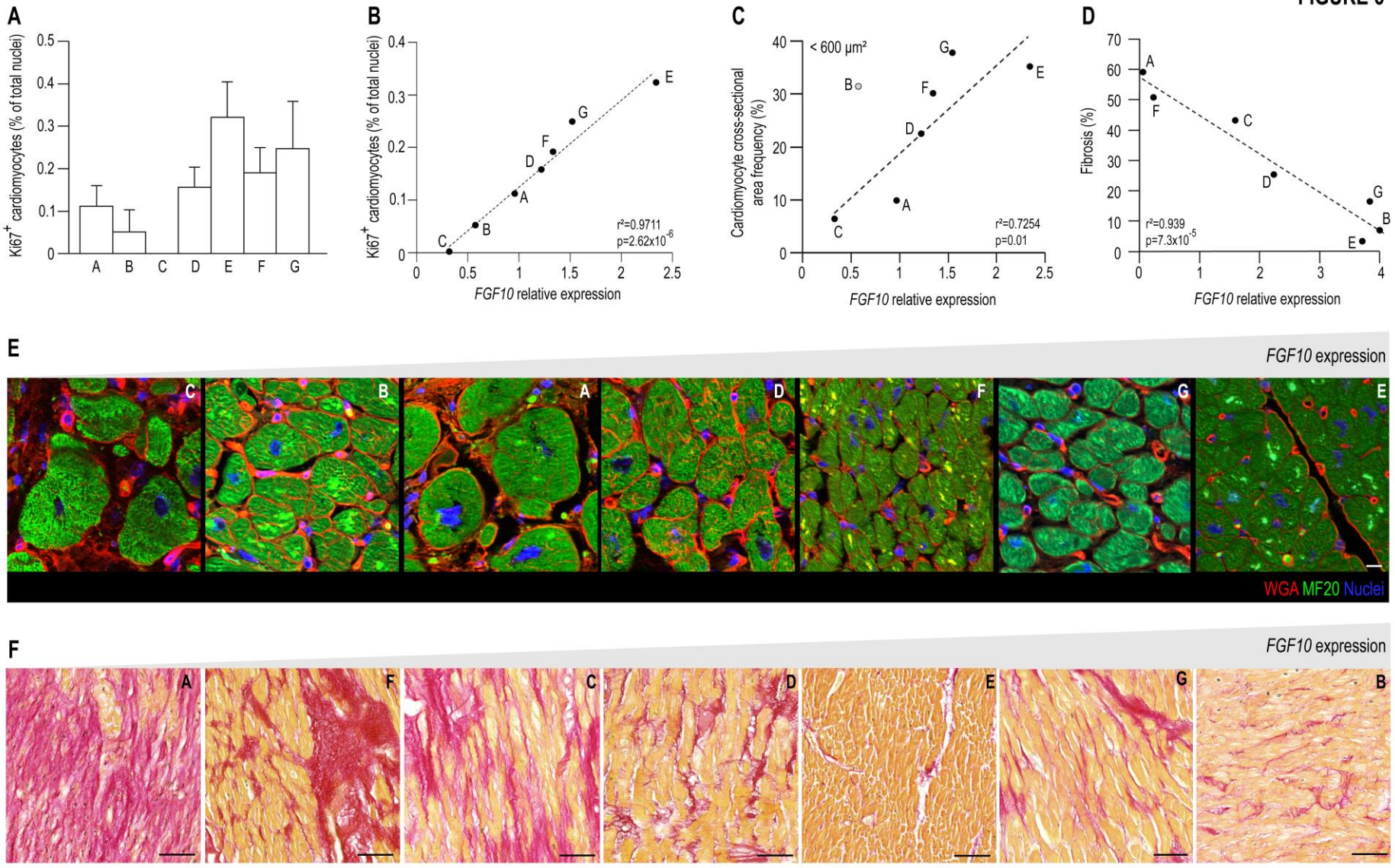
A
Ki67+ cardiomyocytes (% of total nuclei)
0.5
0.4
0.3
0.2
0.1
0
A B C D E F G
B
Ki67+ cardiomyocytes (% of total nuclei)
0.4
0.3
0.2
0.1
0
0 0.5 1 1.5 2 2.5
FGF10 relative expression
r²=0.9711
p=2.62x10-6
C
Cardiomyocyte cross-sectional area frequency (%)
40
30
20
10
0
< 600 µm²
0 0.5 1 1.5 2 2.5
FGF10 relative expression
r²=0.7254
p=0.01
D
Fibrosis (%)
70
60
50
40
30
20
10
0
0 1 2 3 4
FGF10 relative expression
r²=0.939
p=7.3x10-5
E
FGF10 expression
WGA MF20 Nuclei
F
FGF10 expression

Supplemental Figure 1

Click here to access/download;Figure(s);Suppl1.tif

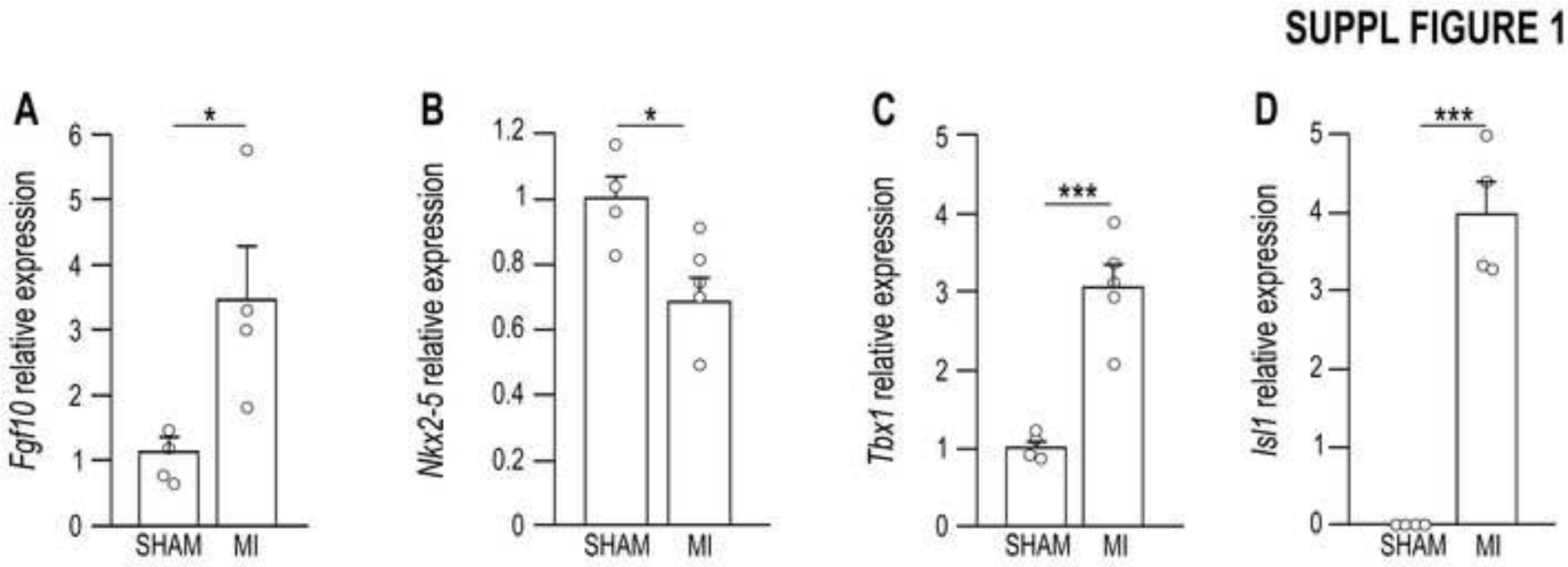

Supplemental Figure 2

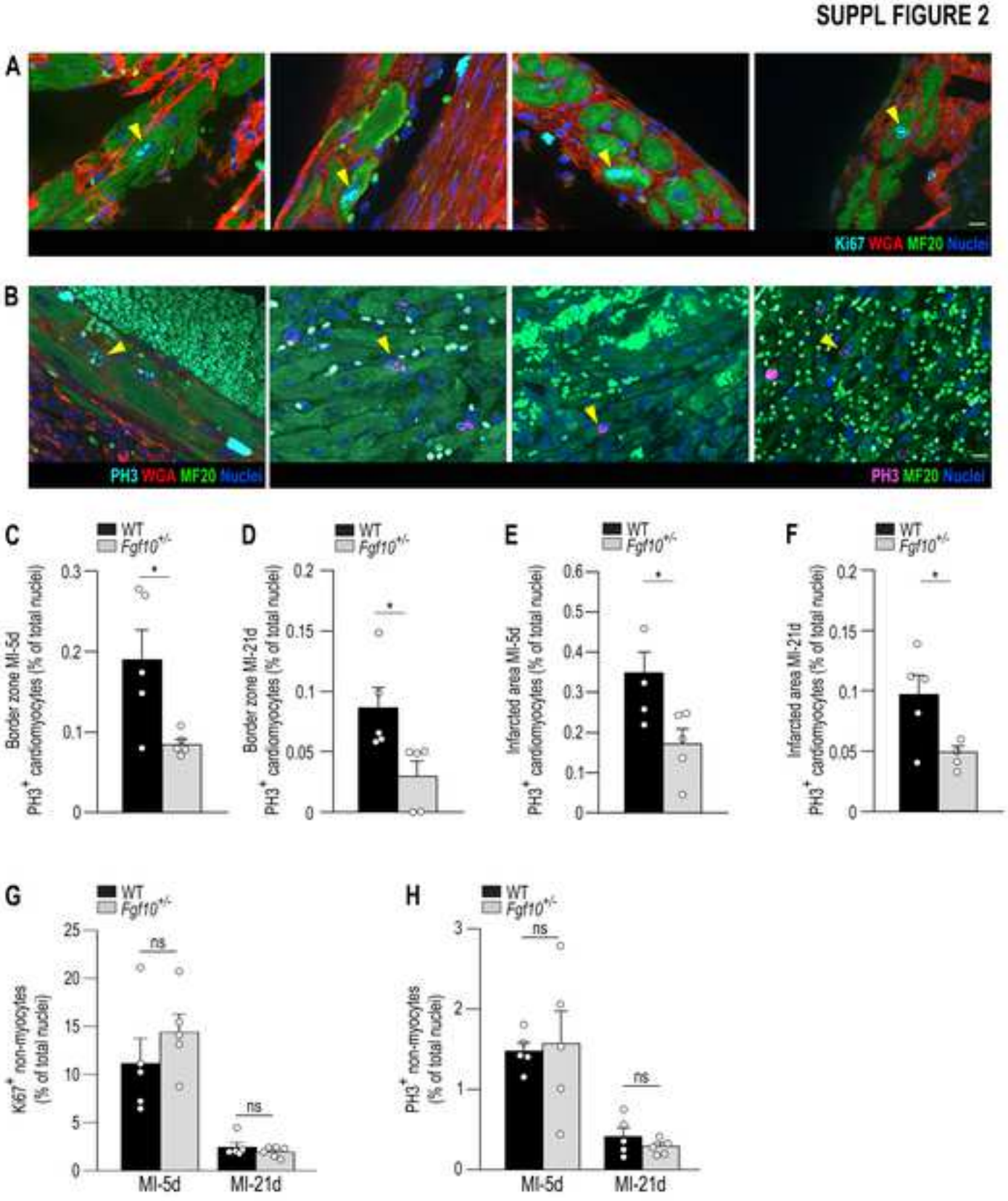

Supplemental Figure 3

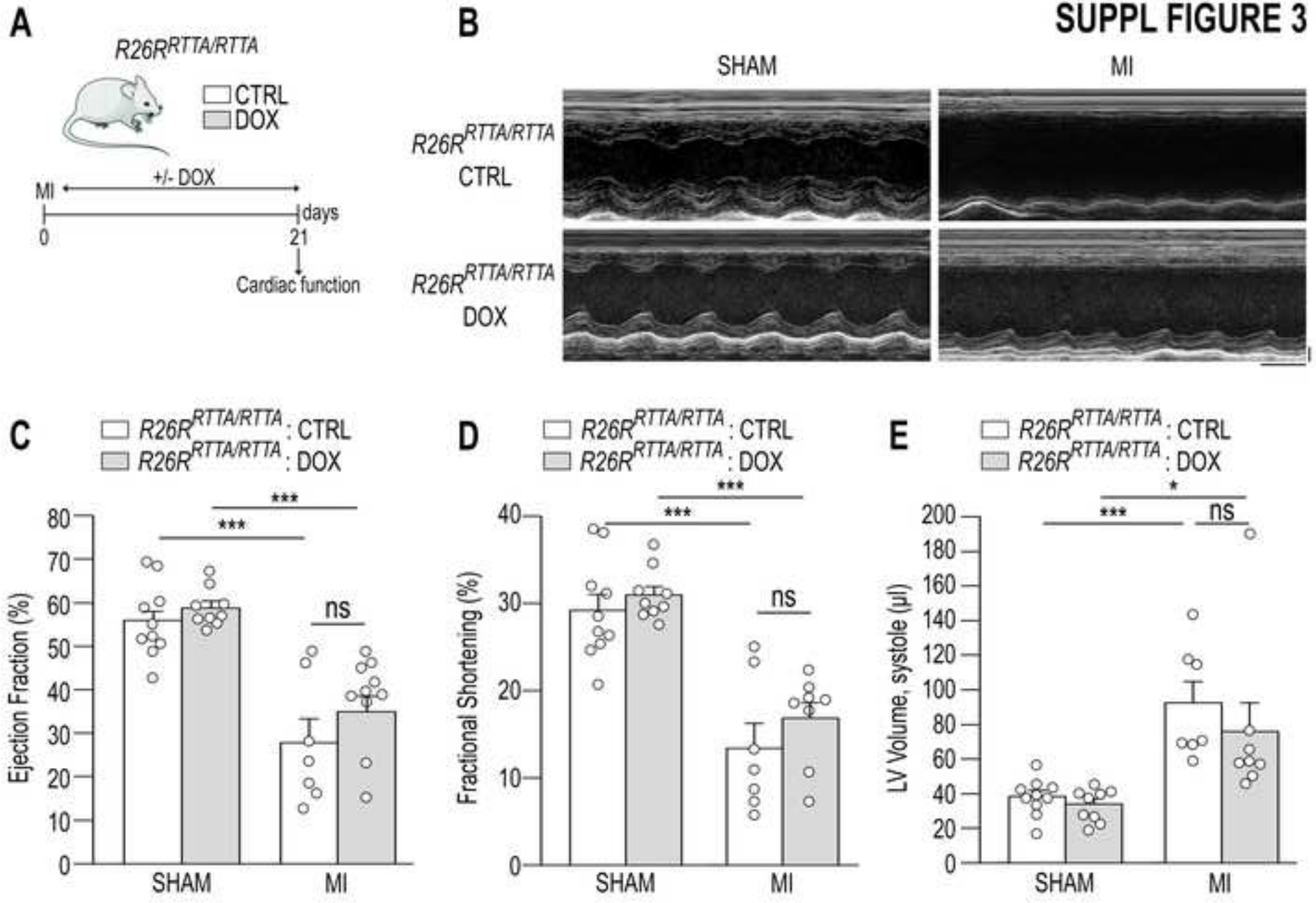

Supplemental Figure 4

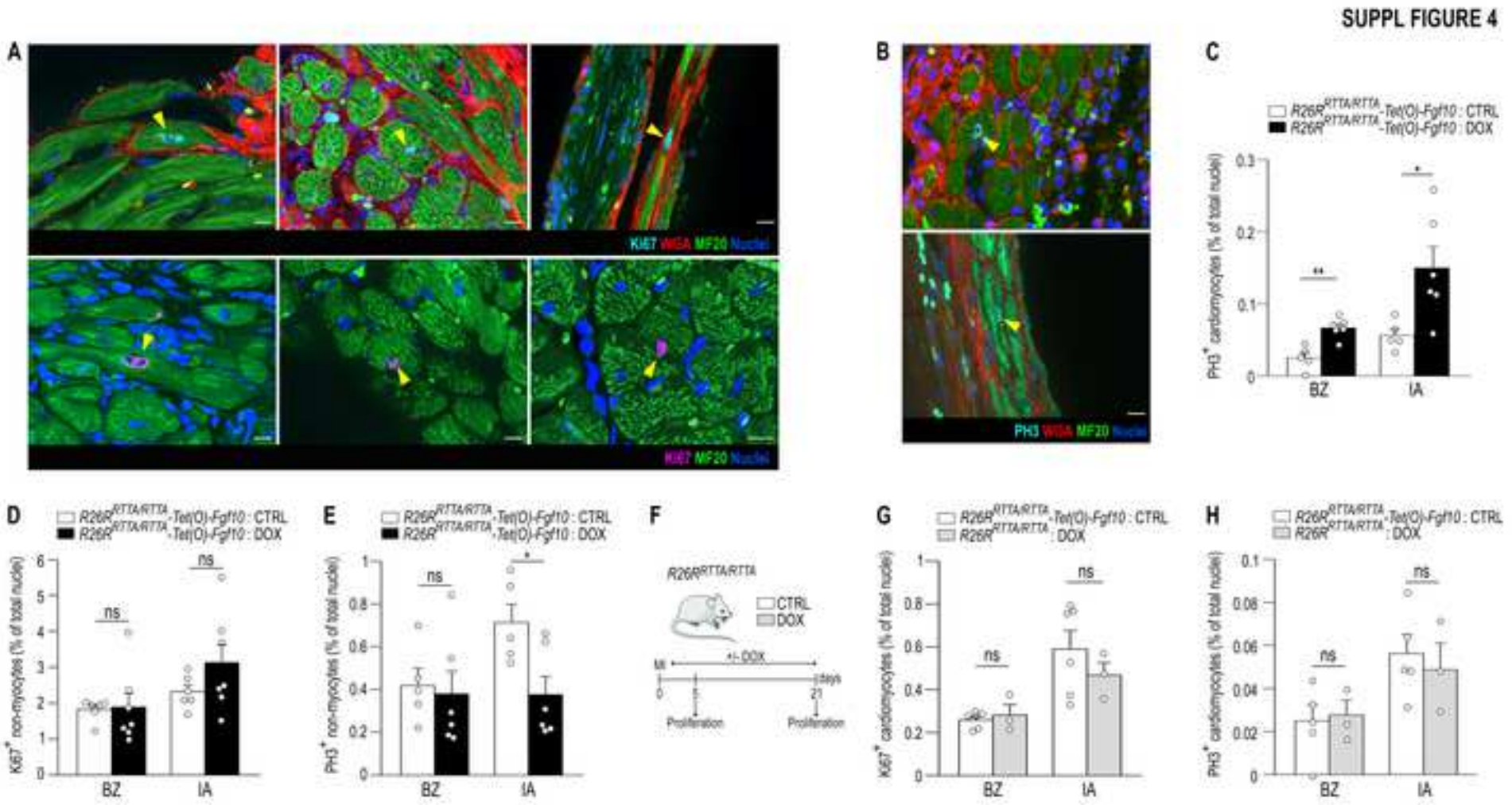

Supplemental Figure 5

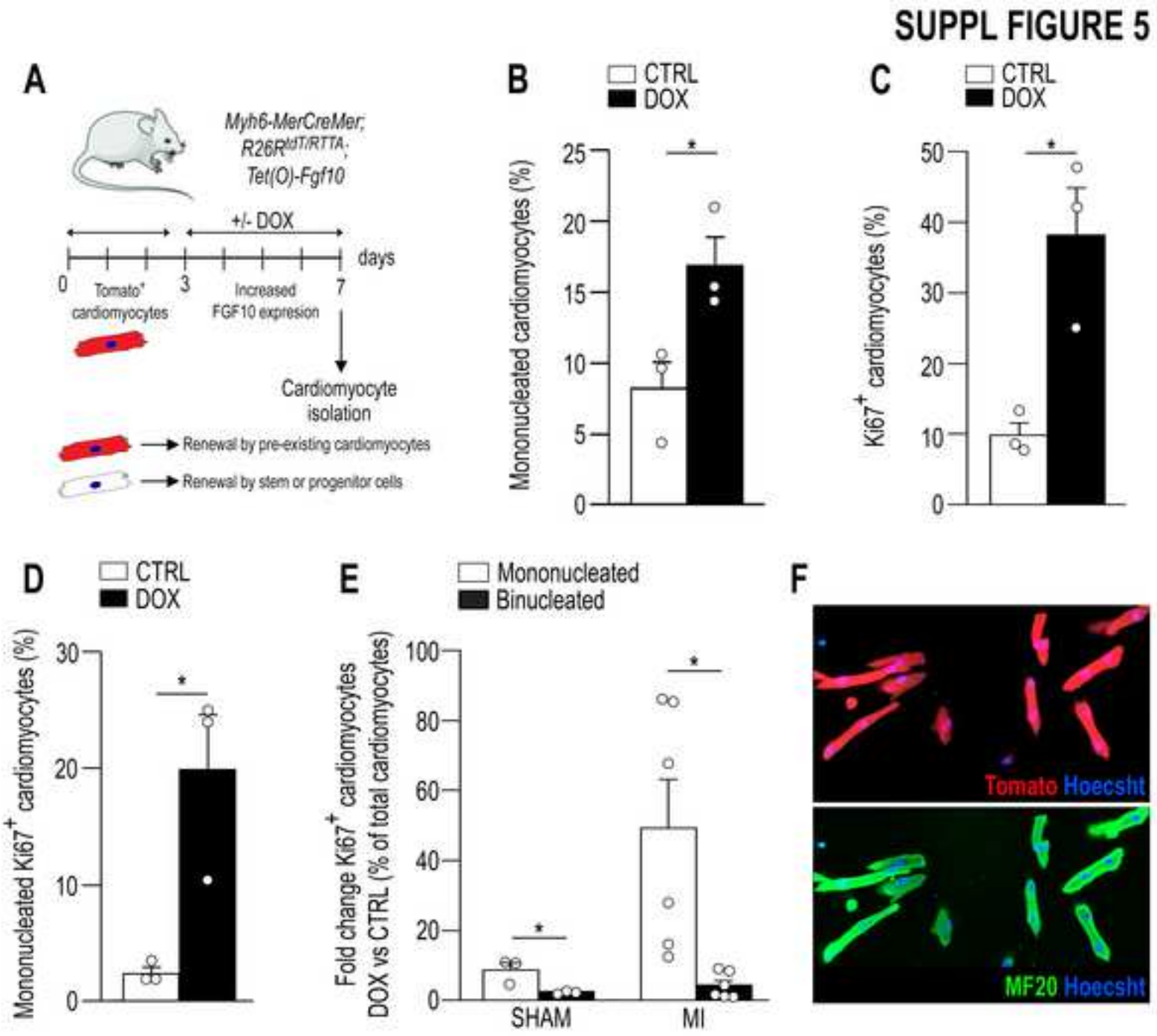

Supplemental Figure 6

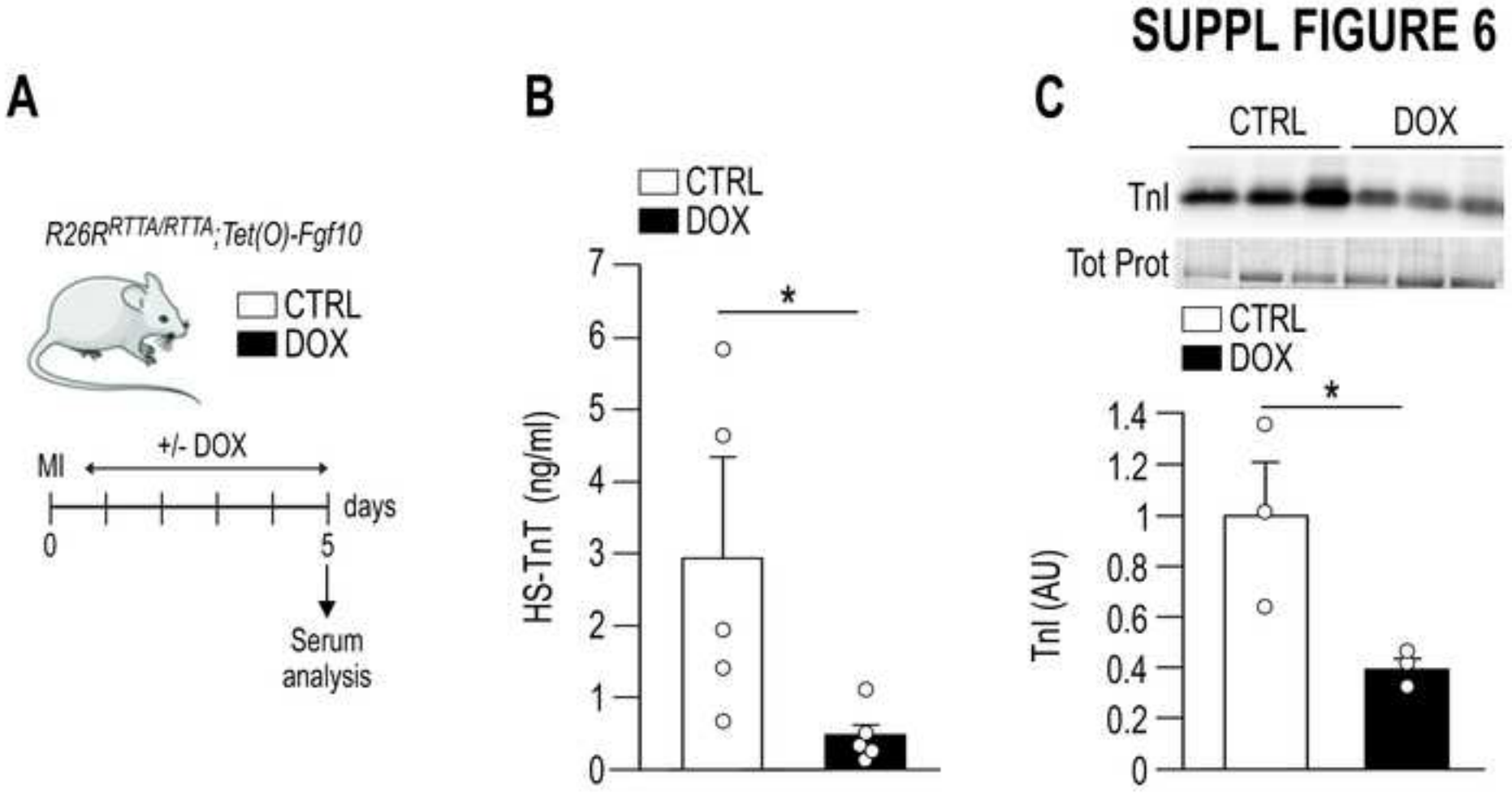

Supplemental Figure 7

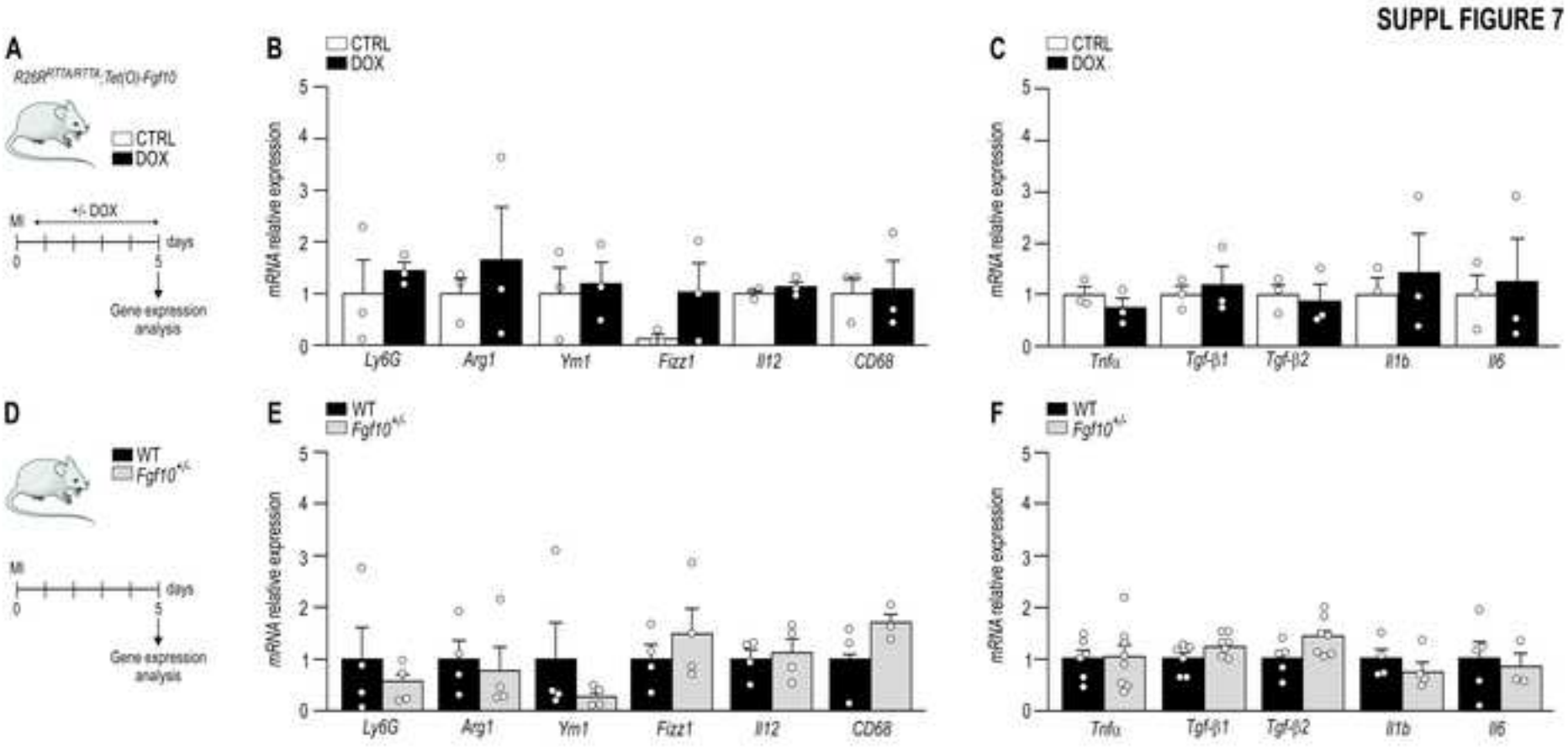

Supplemental Figure 8

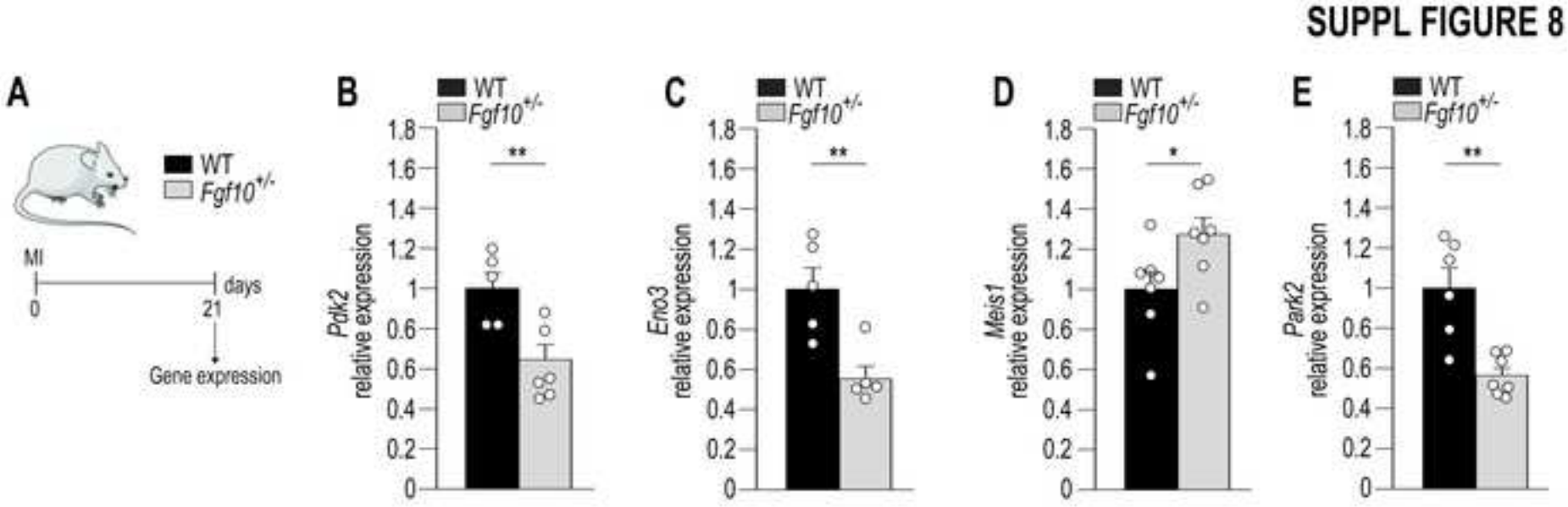

Supplemental Figure 9

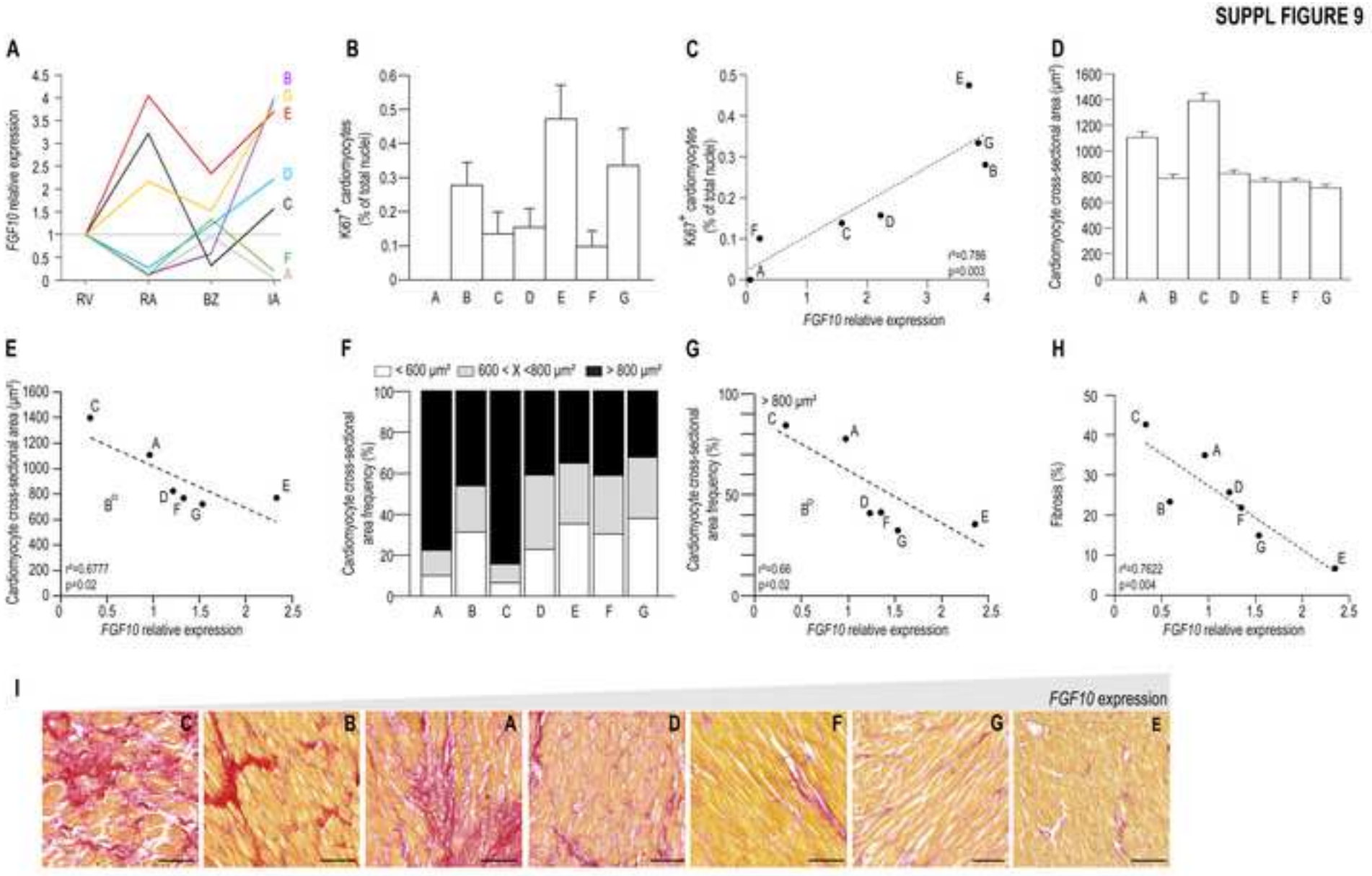

Graphical abstract

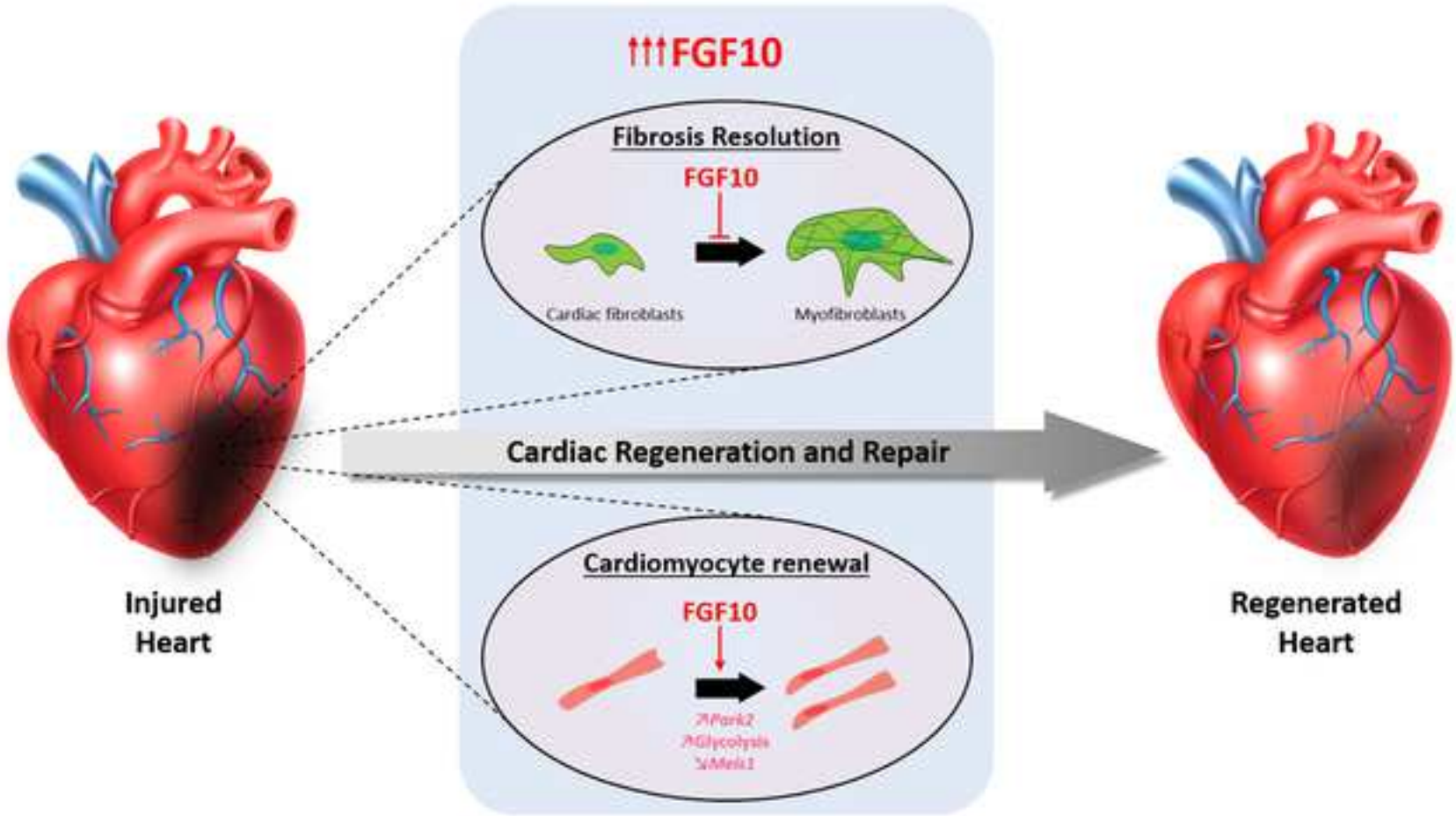

CVR-2021-0222

FGF10 promotes cardiac repair through a dual cellular mechanism increasing cardiomyocyte renewal and inhibiting fibrosis

Fabien Hubert PhD [1#], Sandy M Payan PhD [1#], Edeline Pelce MD-MSc [1,2], Laetitia Bouchard MSc [1], Rachel Sturny [3], Nicolas Lenfant PhD [1], Giovanna Mottola PhD [4,5], Frédéric Collart MD [2], Robert G Kelly PhD [3] and Francesca Rochais PhD [1]

[1] Aix Marseille Univ, INSERM, MMG, U 1251, Marseille, France.

[2] Department of Cardiac Surgery, Timone Hospital, AP-HM, Marseille, France.

[3] Aix Marseille Univ, CNRS UMR 7288, IBDM, Marseille, France.

[4] Aix-Marseille Univ, C2VN, INSERM 1263, INRAE 1260, Marseille, France.

[5] Laboratory of Biochemistry, Timone Hospital, Marseille, France.

# These authors contributed equally

Address for correspondence

Dr. Francesca Rochais, Aix Marseille Université, MMG U1251

27 Boulevard Jean Moulin, 13005 Marseille, France

Phone : +334 91 32 48 86 ; FAX : +334 91 79 72 27

francesca.rochais@univ-amu.fr

SUPPLEMENTARY MATERIAL ONLINE

ONLINE SUPPLEMENTAL METHODS

Mice. The genotyping PCR steps include pre-denaturation at 94°C for 5 minutes, 30 cycles of denaturation (94°C for 45 seconds), annealing (60°C for 45 seconds) and extension (72°C for 45 seconds) followed by a final extension step at 72°C for 7 minutes. PCR products were separated using agarose gel electrophoresis to detect the specific amplified fragments. Primers for genotyping are listed in **Table 1**.

Mouse line	Primer	Sequence (5' - 3')
Fgf10$^{+/-}$	WT-FOR	CTTCCAGTATGTTCCTTCTGATGAGAC
	Mut-FOR	TACGGACAGTCTTCTTCTTGGTCCC
	REV	GAGCTTGCTGGGGGAAACTTCCTGACTAGG
Fgf10-LacZ	FOR	ATCCTCTGCATGGTCAGGTC
	REV	CGTGGCCTGATTCATTCC
Rosa26-rtTA	WT-FOR	AAGTCGCTCTGAGTTGTTATCAG
	WT-REV	GGAGCGGGAGAAATGGATATGA
	Mut-REV	CGGGTTGTTAAACCTTCGATTCCG
Tet(O)-Fgf10	FOR	GACGCCATCCACGCTGT
	REV	TGCTGCCAGTTAAAAGATGC
Rosa26-tdT	WT-FOR	AAGGGAGCTGCAGTGGAGTA
	WT-REV	CCGAAAATCTGTGGGAAGTC
	Mut-FOR	CTGTTCCTGTACGGCATGG
	Mut-REV	GGCATTAAAGCAGCGTATCC

αMHC-MerCreMer	FOR	AGGTTCGTTCACTCATGGA
	REV	TCGACCAGTTTAGTTACCC

Table 1: Genotyping PCR primer sequences.

Sirius red staining. Serial 13 µm sections were obtained and mounted on poly-lysine-treated slides. After dewaxing (xylene, 2 times) and rehydration in an ethanol series (100, 90, 70, 50% and H_2O), paraffin sections were incubated in a 0.1% Sirius Red solution dissolved in saturated aqueous solution of picric acid for 1 hour at room temperature. Subsequently, sections were washed 3 times in acidified water (0.5% acetic acid), dehydrated in ascending concentrations of ethanol (70%, 90% and 100%) and cleared in xylene. Sections were mounted in resinous medium (Entellan). Collagen and non-collagen components were red- and orange-stained, respectively.

Immunofluorescence. Serial 13 µm paraffin sections were obtained and mounted on slides. After dewaxing (xylene, 2 times) and rehydration in an ethanol series (100, 90, 70, 50% and H_2O), antigen was retrieved by boiling samples in Vector Antigen Unmasking Solution (Vector Laboratories, H-3300) for 15 min. Slides were allowed to cool to room temperature for 20 min and washed in PBS-Tween 0.05% (PBST). For blocking, samples were incubated for at least 1 hour in TNB (0.1M Tris-HCl, 0.15M NaCl, 0.5% (w/v)) blocking reagent (PerkinElmer FP1020) prior to incubation with antibodies in TNB overnight at 4°C. This was followed by 3 times PBS-T washes. Slides were then incubated with secondary antibody diluted in TNB for 1 hour at room temperature, followed by 3 washes in PBST and nuclei were counterstained with Hoescht (1/1000) and mounted using FluoroMount (Southern Biotech). Sections were imaged using a Zeiss AxioImager fluorescent microscope with an Apotome module.

Serial 13 µm cryostat sections were obtained from OCT embedded hearts. Sections were kept at room temperature for 15 min to dry and then washed with PBS. Slides were incubated for at least one hour in blocking solution (3% BSA-0.05% Saponin) prior to incubation with primary antibodies in blocking solution overnight at 4°C. This was followed by 3 washes in PBST. Slides were then incubated with secondary antibody in blocking solution for 1 hour at room temperature, followed by 3 washes in PBST. Nuclei were counterstained with Hoescht (1/1000) and mounted with FluoroMount (Southern Biotech). Sections were imaged using a Zeiss AxioImager fluorescent microscope with an Apotome module.

Cells attached onto coverslips were rinsed once in phosphate-buffered saline solution (PBS) for 5 min, fixed in paraformaldehyde 4% (5 min) and washed in PBS (3 times 5 min). The cells were then permeabilized in Triton X-100 0.5% (15 min), washed in PBS (2 times 5 min) and once in PBS-BSA 1% (5 min). Next, they were incubated 1 hour at 37°C with primary antibodies. After three washes in PBS and one in PBS-BSA 1%, the cells were revealed incubated with secondary antibodies (30 min, 37 °C). After three additional washes in PBS, nuclei were counterstained with Hoescht (1/1000) and the coverslips were mounted with FluoroMount (Southern Biotech) and then imaged using a Zeiss AxioImager fluorescent microscope with an Apotome module. Primary and secondary antibodies are listed in **Table 2.**

Primary antibodies			
α-actinin	Mouse	1/500	Sigma A7811
AURKB	Rabbit	1/400	Abcam ab2254
Caspase 3	Rabbit	1/100	Cell signalling 9665
β-galactosidase	Rabbit	1/500	MP Biomedicals 0855976
β-galactosidase	Chicken	1/1000	Abcam ab9361

Ki67	Rabbit	1/100	Abcam ab15580
MF20 sarcomeric myosin heavy chain	Mouse	1/50	DSHB
Phospho Histone H3	Rabbit	1/400	Upstate cell signalling 06-570
WGA-AlexaFluor555		1/50	Thermofisher W32464.
Secondary antibodies			
Anti-Rabbit Alexa Fluor 488	Donkey	1/500	ThermoFisher A-21206
Anti-Mouse Alexa Fluor 488	Donkey	1/500	ThermoFisher A-21202
Anti-Mouse Alexa Fluor 647	Donkey	1/500	ThermoFisher A-31571
Anti-Rabbit Alexa Fluor 647	Donkey	1/500	ThermoFisher A-21208

Table 2: Primary and secondary antibodies.

Quantitative Real Time PCR. Quantitative RT-PCR primers are listed in **Table 3**.

Gene	Species	Primer	Sequence (5' - 3')
Acta2	mouse human	Acta2-F	ACTCTCTTCCAGCCATCTTTCA
		Acta2-R	ATAGGTGGTTTCGTGGATGC
Angpt1	mouse	Angpt1-F	GGAAGATGGAAGCCTGGAT
		Angpt1-R	ACCAGAGGGATTCCCAAAAC
Ccnk	mouse	Ccnk-F	GTTTGGAGATGACCCAAAGG
		Ccnk-R	AAGTCAAACTTTATGGTCTGCAGTAA
Cdkn2b	mouse	Cdkn2b-F	AATAACTTCCTACGCATTTTCTGC
		Cdkn2b-R	CCCTTGGCTTCAAGGTGAG
Col1A1	mouse	Col1A1-F	CATGTTCAGCTTTGTGGACCT

		Col1A1-R	GCAGCTGACTTCAGGGATGT
Col3A1	mouse	Col3A1-F	TGGTCCTGCTGGAAAGGAT
		Col3A1-R	GAGGTCCAGGCAGTCCAC
Col6A5	mouse	Col6A5-F	CCTCCTGGTCGGAGAGGT
		Col6A5-R	TTCACAGGGGGAATATATAGGTTG
Crispld2	mouse	Crispld2-F	AGGTTGAGGCCAGAGTTCC
		Crispld2-R	GCCTTCAGCCACAACTAAGAG
Ddr2	mouse	Ddr2-F	ATGTTGGCAGGCAAGACAG
		Ddr2-R	TCAGGTCGCTTGTAGATTTCC
Efnb3	mouse	Efnb3-F	TGGAACTCGGCGAATAAGAG
		Efnb3-R	CCCCGATCTGAGGATAAAGC
Eno3	mouse	Eno3-F	ACACAGCCAAGGGTCGATT
		Eno3-R	TCCACAGCCTTCAGCACTC
Erbb3	mouse	Erbb3-F	CACGAGAACTGCACCCAAG
		Erbb3-R	TCTGCTTGGCCTAAACAGTCT
Fgf10	mouse rat	Fgf10-F	GAGAAGAACGGCAAGGTCAG
		Fgf10-R	TTTCCCCTTCTTGTTCATGG
	human	FGF10-F	GAAGGAGAACTGCCCGTACA
		FGF10-R	GGCAACAACTCCGATTTCTACT
Hprt	mouse	Hprt-F	CTGGTGAAAAGGACCTCTCG
		Hprt-R	TGGCAACATCAACAGGACTC
Homer2	mouse	Homer2-F	CCAGAGACAAGTCCCAGGAG
		Homer2-R	CCATTGACGCTGGATGCT

IL-1b	mouse	IL-1b-F	AGTTGACGGACCCCAAAAG
		IL-1b-R	TTTGAAGCTGGATGCTCTCAT
IL-6	mouse	IL-6 F	GATGGATGCTACCAAACTGGAT
		IL-6 R	CCAGGTAGCTATGGTACTCCAGA
Isl1	mouse	Isl1-F	AGCAACCCAACGACAAAACT
		Isl1-R	CCATCATGTCTCTCCGGACT
Mdh1	mouse	Mdh1-F	TGCTCTACTCATTCCCTGTCG
		Mdh1-R	CCTTTGCTGTCAGGTCCATC
Meis1	mouse	Meis1-F	ATGGGTTCCTCGGTCAATG
		Meis1-R	CATTTCTCAAAAATCAGTGCTAAGA
Myh6	mouse	Myh6-F	CCTCAAGCTCATGGCTACAC
		Myh6-R	TTGCCTCCTTTGCCTTTACC
Myh7	mouse	Myh7-F	AGGCAAAGAAAGGCTCATCC
		Myh7-R	TGGAGCGCAAGTTTGTCATA
Nkx2.5	mouse	Nkx2.5-F	CAAGTGCTCTCCTGCTTTCC
		Nkx2.5-R	CTTTGTCCAGCTCCACTGC
Nppa	mouse	Nppa -F	CAACACAGATCTGATGGATTTCA
		Nppa -R	CCTCATCTTCTACCGGCATC
Nppb	mouse	Nppb -F	GTCAGTCGTTTGGGCTGTAAC
		Nppb -R	AGACCCAGGCAGAGTCAGAA
Park2	mouse	Park2-F	CGCGTAGGTCCTTCTCGAC
		Park2-R	GAAAGGCTGGGCCTAGATACA
Pdgfra	mouse	Pdgfra-F	AAGACCTGGGCAAGAGGAAC

		Pdgfra-R	GAACCTGTCTCGATGGCACT
Pdha1	mouse	Pdha1-F	GTAAGGGGCCCATCCTGA
		Pdha1-R	TCTTCTCGAGTGCGGTAGC
Pdhb	mouse	Pdhb-F	TGATGAAGACAAATCATCTCGTG
		Pdhb-R	AGGGGCATCAAGGAAGTTG
Pdk1	rat	Pdk1-F	CCGATTCAAGTTCACGTCAC
		Pdk1-R	ACCTCCCCGGTCACTCAT
Pdk2	mouse	Pdk2-F	TGGCTAAGCTCCTGTGTGAC
		Pdk2-R	CATGTGAATGGGCTGGTTG
Pecam1	mouse	CD31-F	CGGTGTTCAGCGAGATCC
		CD31-R	ACTCGACAGGATGGAAATCA
Pfkm	mouse	Pfkm-F	GGACAATCTGCAAGAAAGCA
		Pfkm-R	TGATGCTCTTCATGGGTCAT
pfkp	mouse	Pfkp-F	GAGGGACCCCATCTGCAT
		Pfkp-R	GTAGCTTCCAGCAAGGCAAT
Ppargc1a	mouse	Ppargc1a-F	AGCCTGCGAACATATTTGAGA
		Ppargc1a-R	ATGAGGGCAATCCGTCTTC
PPIA	Human	PPIA-F	ATGCTGGACCCAACACAAAT
		PPIA-R	TCTTTCACTTTGCCAAACACC
Prkaa2	mouse	Prkaa2-F	CGACTACATCTGCAAACATGG
		Prkaa2-R	CAGTAATCCACGGCAGACAG
Smoc1	mouse	Smoc1-F	GATAAGGTCATCTCACTGCCTGA
		Smoc1-R	AAGCTGCCAAGGCTACCAC

Smoc2	mouse	Smoc2-F	CGTGGGAATTGCAAAGATG
		Smoc2-R	CCTGCTCCTGGGTATACTTCC
Tbx1	mouse	Tbx1-F	TTTGTGCCCGTAGATGACAA
		Tbx1-R	ACTCGGCCAGGTGTAGCA
Tcf7	mouse	Tcf7-F	AGGAGCTGCAGCCATATGAT
		Tcf7-R	TGACTGGCTTCTTAGCCTCCT
TGFb1	mouse	TGFb1-F	TGGAGCAACATGTGGAACTC
		TGFb1-R	GTCAGCAGCCGGTTACCA
TGFb2	mouse	TGFb2-F	AGGAGGTTTATAAAATCGACATGC
		TGFb2-R	TAGAAAGTGGGCGGGATG
TGFb3	mouse	TGFb3-F	CCCTGGACACCAATTACTGC
		TGFb3-R	TCAATATAAAGGGGGCGTACA
Tnfα	mouse	TNFα-F	AGCCTCTTCTCATTCCTGCTT
		TNFα-R	ATGAGAGGGAGGCCATTTG.
Vegfb	mouse	Vegfb-F	GCTCAACCCAGACACCTGTAG
		Vegfb-R	AGGAGGTTCGCCTGTGCT
Vegfc	mouse	Vegfc-F	GAGTCGGGACTGGGCTTC
		Vegfc-R	GACACAGACCGCAACTGCT
YWHAZ	human	YWHAZ-F	GTGGACATCGGATACCCAAG
		YWHAZ-R	AAGTTGGAAGGCCGGTTAAT

Table 3: Quantitative RT-PCR primer sequences.

Data processing and differential gene expression (DGE) analysis.

70 millions of reads (clusters) have been sequenced, on average, by sample. The quality of sequencing reads was assessed using fastQC[1]**.** Reads were mapped to the mouse reference genome (GRCm38/mm10) using STAR (v2.5.3a)[2] and bam files were indexed and sorted using Sambamba (v0.6.6)[3]. Number of read fragments per gene (GENCODE annotations) was determined after mapping using Stringtie (v1.3.1c)[4]. Differential gene expression analysis was performed using DESeq2[5]. p-values were adjusted for multiple testing using the method by Benjamini and Hochberg[6] and genes with an FDR (False Discovery Rate) adjusted p-value below 0.05 were considered as significantly differentially expressed. The heatmap of Differentially Expressed Genes using was generated using the Pheatmap R package, while the volcano plot representing the Log_2FC (log2 of the expression fold change) and the adjusted p-value of the Wald test has been prepared by using the EnhancedVolcano R package. Enrichment (Gene set enrichment Analysis, GSEA) and overrepresentation (Singular Enrichment Analysis, SEA) in GO term analysis were performed using a Mann-Whitney test and hypergeometric test respectively, thanks to the Clusterprofiler R package. In the case of over-representation, the test was set on genes having a FDR adjusted p-value below 0.001, the value commonly accepted as threshold for significance. Results of GSEA and SEA, have been represented, for a set of selected genes, as Circos plot with GOplot R package.

[1]Andrews S. Fastqc: A Quality Control Tool for High Throughput Sequence Data. Available online at https://www.bioinformatics.babraham.ac.uk/projects/fastqc. 2010.

[2]Dobin A and Gingeras TR. Mapping RNA-seq Reads with STAR. Current Protocols in Bionformatics. 2015; 51(1), 11.14.1-11.14.19.

[3]Tarasov A, Vilella AJ, Cuppen E, Nijman IJ and Prins P. Sambamba: fast processing of NGS alignment formats. Bioinformatics. 2015; 31(12): 2032–2034.

[4]Pertea M, Pertea GM, Antonescu CM, Chang TC, Mendell JT and Salzberg SL. StringTie enables improved reconstruction of a transcriptome from RNA-seq reads. Nature Biotechnology. 2015; 33(3), 290–295.

[5]Love MI, Huber W and, Anders S. Moderated estimation of fold change and dispersion for RNA-seq data with DESeq2. Genome Biol. 2014; 15(12): 550.

[6]Benjamini Y and Hochberg Y. Controlling the false discovery rate: a practical and powerful approach to multiple testing. J R Stat Soc B. 1995; 57, 289-300.

ONLINE SUPPLEMENTAL FIGURES

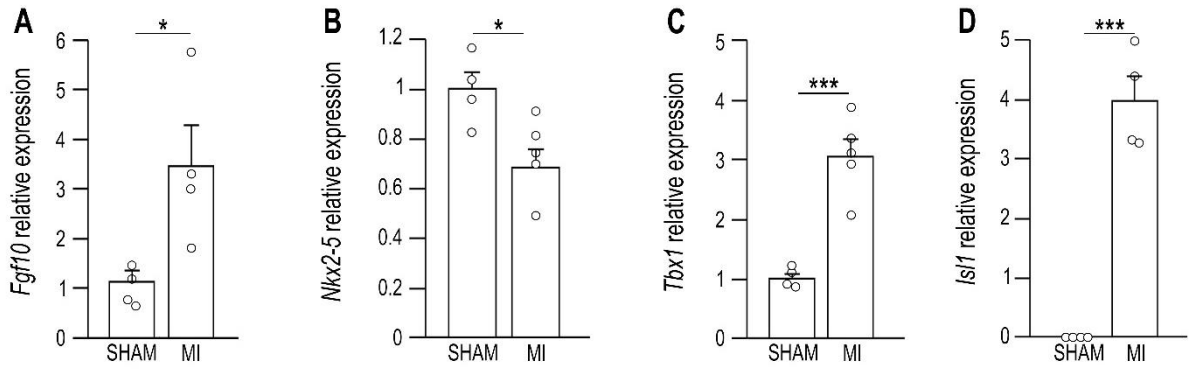

Supplemental Figure 1: *Fgf10* expression is upregulated after myocardial infarction (MI). qRT-PCR experiments on left ventricular MI hearts showing (**A**) *Fgf10*, (**B**) *Nkx2*-5, (**C**) *Tbx1* and (**D**) *Isl1* expression 21 days after MI (n=4-5 per group). *Isl1* expression is normalized to right ventricular expression. *, p<0.05; ***, p<0.001; Student's *t*-test.

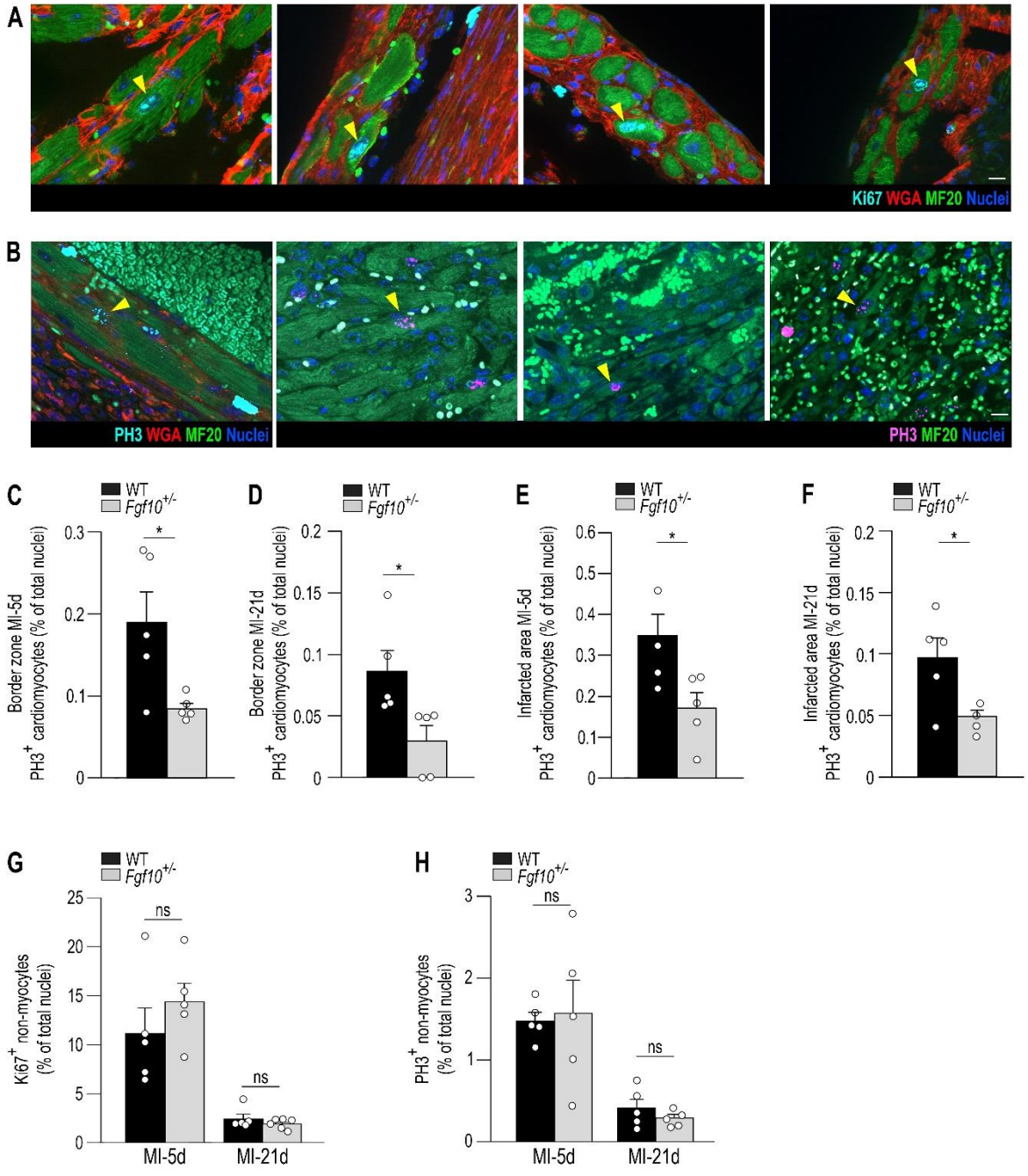

Supplemental Figure 2: Decreased *Fgf10* dosage impairs maximal cardiomyocyte proliferation post-MI. WT and *Fgf10*$^{+/-}$ adult mice were subjected to myocardial infarction. Immunofluorescence experiments on paraffin sections were performed to evaluate, in the border zone, *in vivo* cardiomyocyte proliferation (MF20^{+}; yellow arrowheads) post-MI using Ki67 (**A**) and PH3 (**B**). Border zone *in vivo* cardiomyocyte proliferation (PH3^{+}MF20^{+}; yellow arrowheads) 5 days (**C**; n=5/group) and 21 days (**D**; n=5/group) post-MI. Infarcted area *in vivo* cardiomyocyte proliferation (PH3^{+}MF20^{+}; yellow arrowheads) 5 days (**E**; MI-5d; n=5/group) and 21 days (**F**; MI-21d; n=5/group) post-MI. *In vivo* non-myocyte proliferation (MF20^{-}), in the border zone, was determined 5 (WT, n=5; *Fgf10*$^{+/-}$, n=5) and 21 (WT, n=5; *Fgf10*$^{+/-}$, n=6) days post-MI using Ki67 (**G**) and PH3 (**H**). Scale bars 10 µm. ns, non-significant; *, p<0.05; Student's t-test.

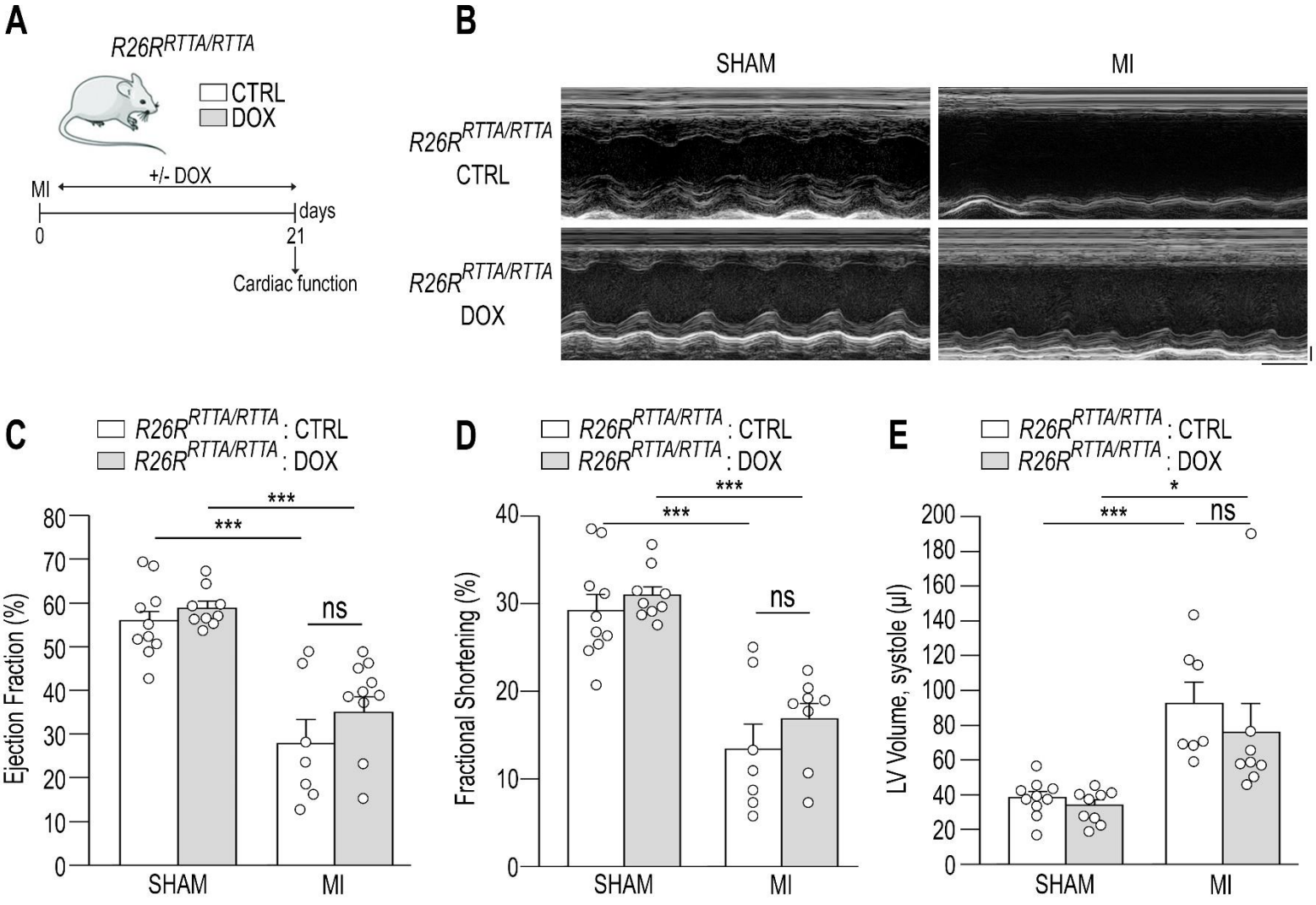

Supplemental Figure 3: Upregulation of *Fgf10* levels post-MI preserves cardiac function and remodeling. (A) Schematic of the experimental plan. *R26R-RTTA* mice were subjected to myocardial infarction (MI). One day after MI, mice were fed with normal (CTRL) or doxycycline supplemented food (DOX). (**B**) M-mode images of echocardiographic experiments (Scale bars, x: 0.1 s; y: 1 mm). (**C**) Ejection fraction, (**D**) fractional shortening and (**E**) left ventricular systolic volume. SHAM-CTRL, n=10; SHAM-DOX, n=9; MI-CTRL, n=7; MI-DOX, n=8. ns, non-significant; *, p<0.05; ***, p<0.001; Student's *t*-test.

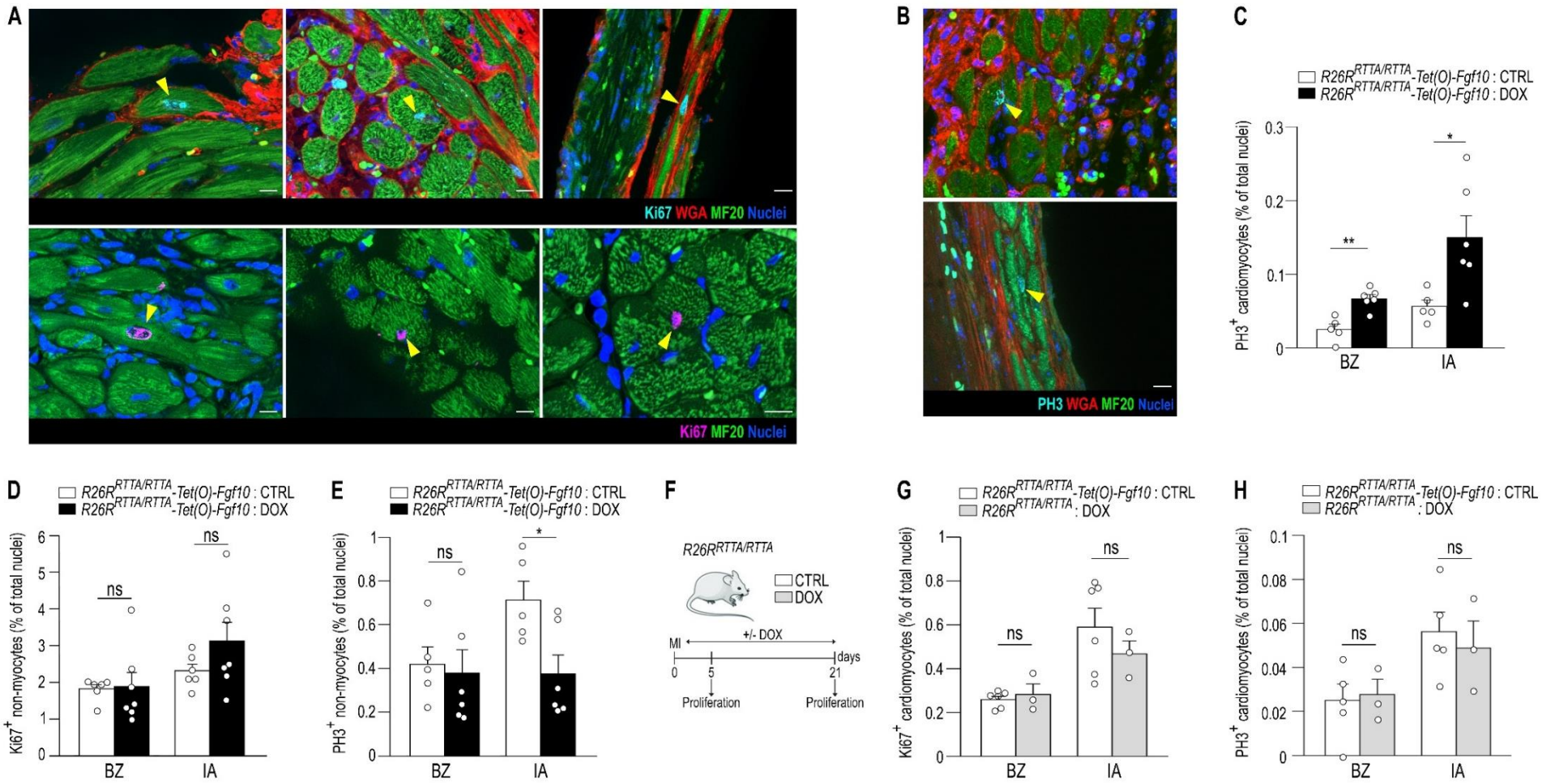

Supplemental Figure 4: Upregulation of *Fgf10* levels post-MI promotes cardiomyocyte cell cycle reentry. (**A-E**) *R26R-RTTA/Tet(O)-Fgf10* mice were subjected to myocardial infarction (MI). One day after MI, mice were fed with normal (CTRL) or doxycycline (DOX) supplemented food. Immunofluorescence experiments on paraffin sections were performed 21 days post-MI to evaluate cell proliferation in the border zone (BZ) and in the infarcted area (IA). Cardiomyocyte proliferation was detected using Ki67 (**A**) and PH3 markers (**B-C;** *R26R-RTTA/Tet(O)-Fgf10*:CTRL n=5; *R26R-RTTA/Tet(O)-Fgf10*:DOX n=6). Scale bars: 10 µm. (**D-E**) Non-myocyte proliferation was detected by Ki67$^+$ (**D**; *R26R-RTTA/Tet(O)-Fgf10*:CTRL n=6; *R26R-RTTA/Tet(O)-Fgf10*:DOX n=7) and PH3 (**E**, *R26R-RTTA/Tet(O)-Fgf10*:CTRL n=5; *R26R-RTTA/Tet(O)-Fgf10*:DOX n=6) markers. (**F-H**) *R26R-RTTA* mice were subjected to myocardial infarction (MI). One day after MI, mice were fed with normal (CTRL) or doxycycline (DOX) supplemented food. Immunofluorescence experiments on paraffin sections were performed, 21 days post-MI, to evaluate cell proliferation in the border zone (BZ) and in the infarcted area (IA; *R26R-RTTA/Tet(O)-Fgf10*:CTRL n=6, *R26R-RTTA*:DOX n=3). ns, non-significant; *, p<0.05; **, 0,001<p<0.01; Student's *t*-test.

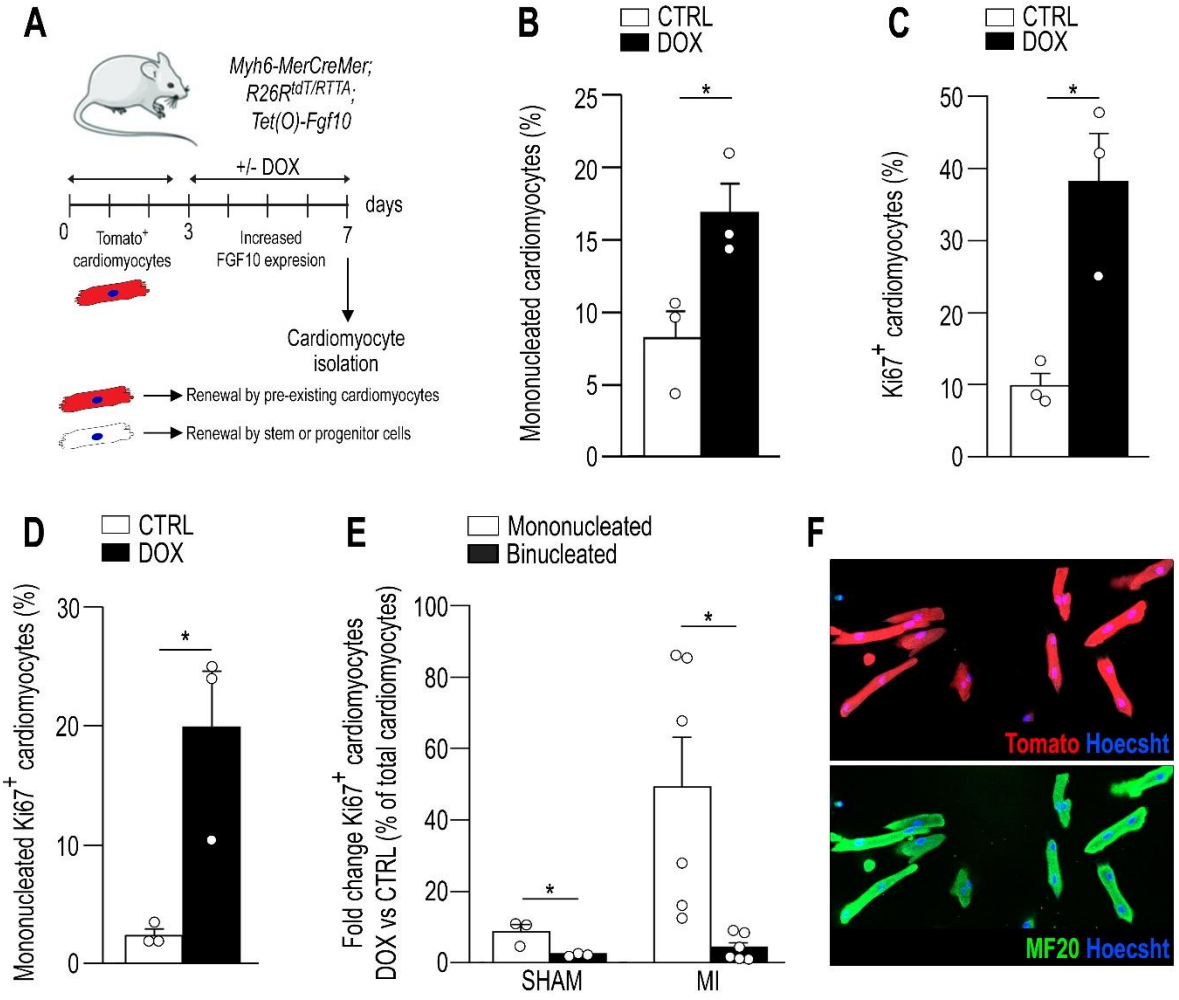

Supplemental Figure 5: Upregulation of *Fgf10* levels promotes cardiomyocyte renewal. (**A**) *αMHC-MerCreMer/R26R-tdT/R26R-RTTA/Tet(O)-Fgf10* mice were injected with Tamoxifen (Tam) and then fed with doxycycline (DOX) supplemented food for 5 days. (**B-D**) Cardiomyocytes were isolated and immunofluorescence experiments were performed to evaluate mononucleated cardiomyocyte proliferative capacities. (**E**) Cardiomyocytes were isolated and immunofluorescence experiments were performed to evaluate mono- and binucleated cardiomyocyte proliferative capacities in normal (SHAM; n=3) and myocardial infarction (MI; n=6) conditions. (**F**) Cardiomyocytes were isolated and immunofluorescence experiments were performed to evaluate cardiomyocyte lineage.

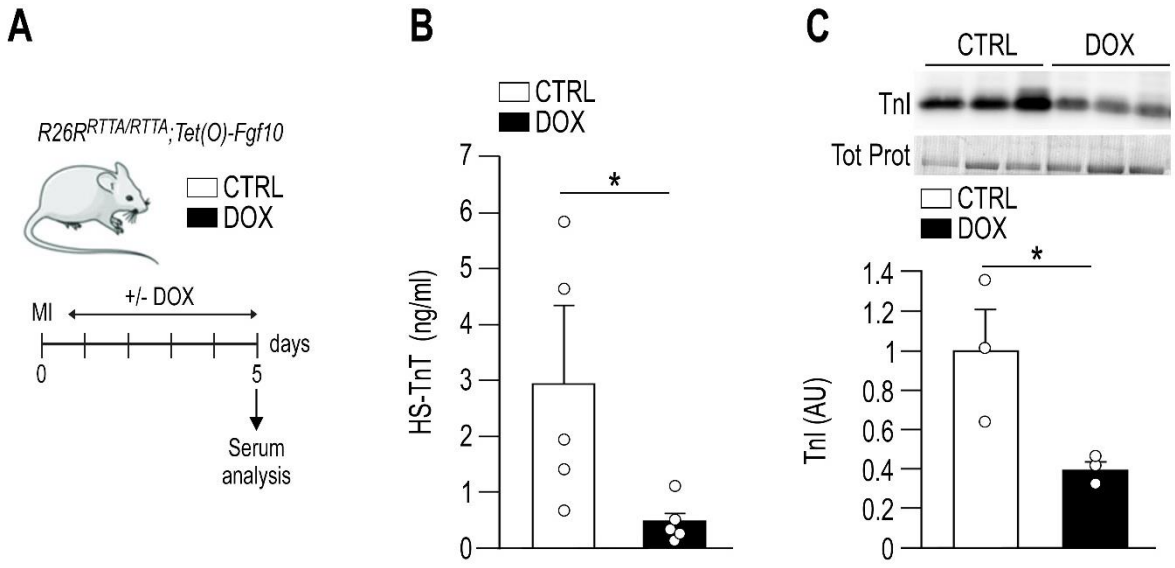

Supplemental Figure 6: Upregulation of *Fgf10* levels post-MI prevents cardiomyocyte cell death. (**A**) *R26R-RTTA/Tet(O)-Fgf10* mice were subjected to myocardial infarction (MI). One day after MI, mice were fed with normal (CTRL) or doxycycline (DOX) supplemented food for 5 days. (**B**) High-sensitive cardiac troponin T (HS-TnT) serum level analysis (n=5 per group). (**C**) Western blot experiment revealing reduced cardiac Troponin I (TnI) serum levels in DOX-compare to CTRL-treated animals post-MI (n=3 per group). *, $p<0.05$; Student's *t*-test.

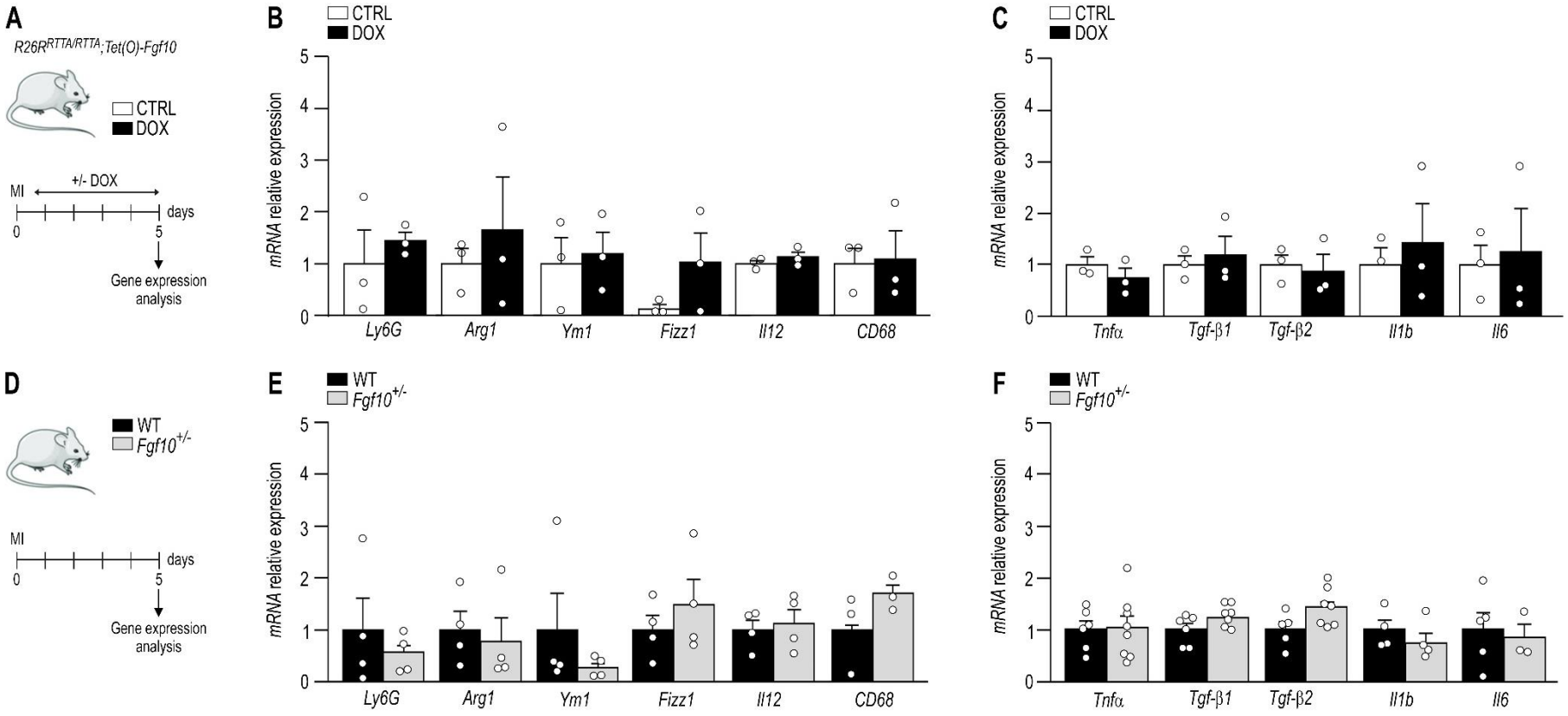

<u>Supplemental Figure 7</u>: Impact of modulated *Fgf10* expression on myocardial inflammation post-MI. (**A-C**) *R26R-RTTA/Tet(O)-Fgf10* mice were subjected to myocardial infarction (MI). One day after MI, mice were fed with normal (CTRL) or doxycycline (DOX) supplemented food for 5 days. qRT-PCR analysis of key inflammatory cell (**B**) and cytokine (**C**) gene expression in the infarcted area 5 days post-MI. n=3-8 per group. (**D-F**) WT and *Fgf10*$^{+/-}$ adult mice were subjected to myocardial infarction. qRT-PCR analysis of key inflammatory cell (**E**) and cytokine (**F**) gene expression in the infarcted area 5 days post-MI. n=3-8 per group.

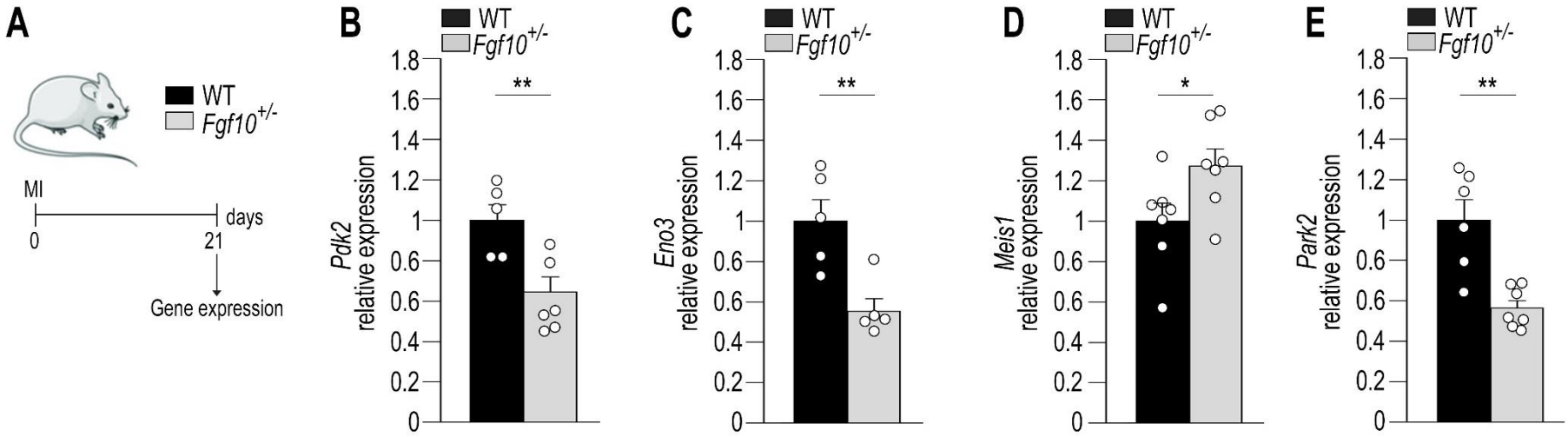

<u>Supplemental Figure 8:</u> Impact of decreased *Fgf10* dosage on *Pdk2*, *Eno3*, *Mesi1* and *Park2* expression following MI. (**A**) Schematic of the experimental plan. WT and *Fgf10*$^{+/-}$ adult mice were subjected to myocardial infarction (MI) and analysis were performed 21 days after surgery. qRT-PCR analysis 21 days post-MI of (**B**) *Pdk2* (WT, n=5; *Fgf10*$^{+/-}$, n=6), (**C**) *Eno3* (WT, n=5; *Fgf10*$^{+/-}$, n=5), (**D**) *Meis1* (WT, n=7; *Fgf10*$^{+/-}$, n=7) and (**E**) *Park2* (WT, n=6; *Fgf10*$^{+/-}$, n=7) expression in the infarcted area. ns, non-significant; *, p<0.05; **, 0,001<p<0.01; Student's *t*-test.

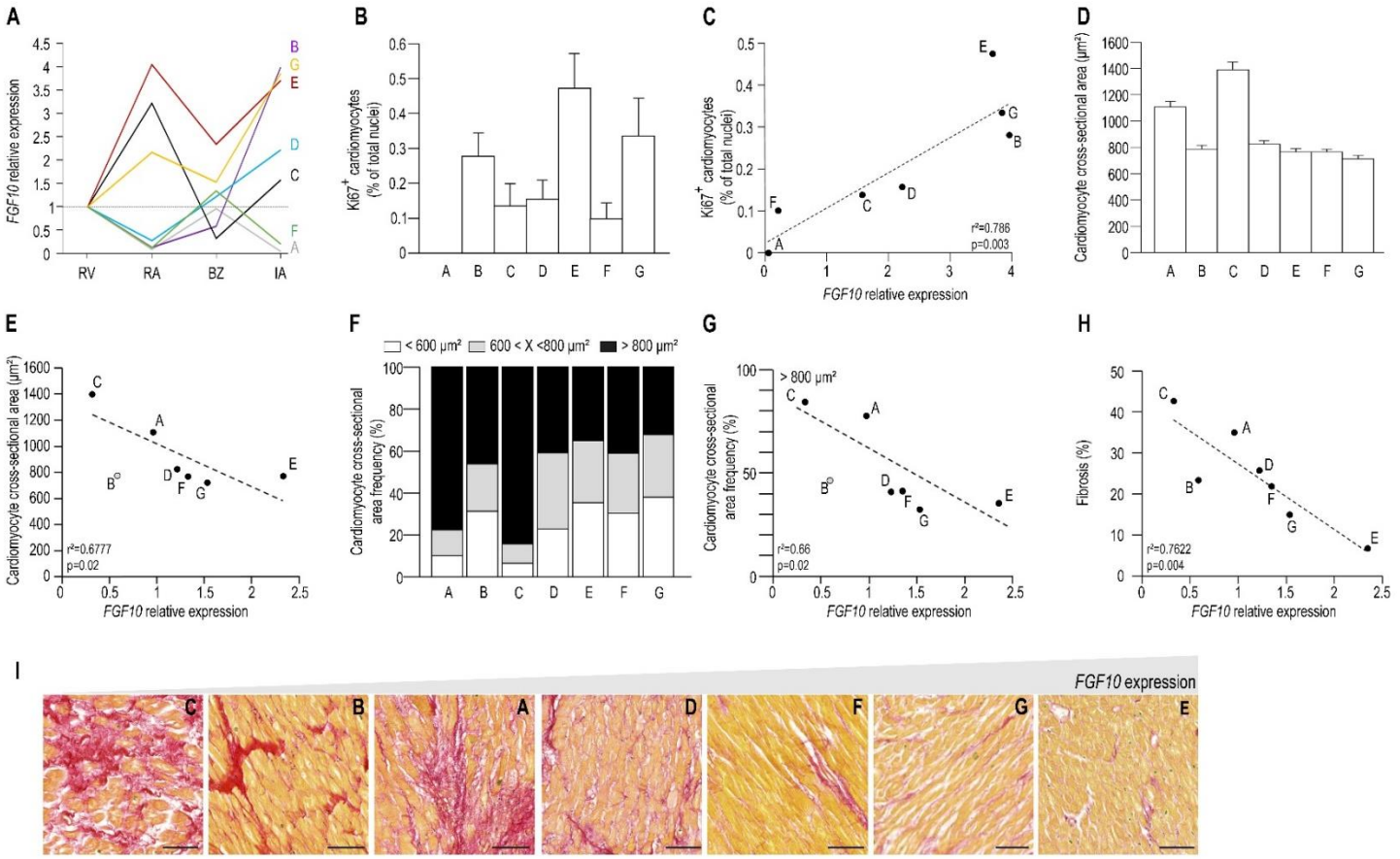

<u>Supplemental Figure 9</u>: *FGF10* upregulated levels in human failing heart correlate with increased cardiomyocyte proliferation, reduced cardiomyocyte size and reduced fibrosis. Human explanted failing heart samples from right ventricle (RV), remote area (RA), border zone (BZ) and infarcted area (IA) were collected from 7 patients (A-G). (**A**) qRT-PCR experiments revealed upregulated *FGF10* levels in the BZ (4 patients out of 7) and the IA (5 patients out of 7). (**B**) Cardiomyocyte proliferation in the infarcted area was evaluated using immunofluorescence experiments on paraffin sections and the cell cycle marker Ki67. (**C**) Elevated *FGF10* levels correlate with enhanced cardiomyocyte proliferation in the IA (r^2=0.786, p=0.003). (**D**) Cardiomyocyte cross-sectional area measurement in the border zone using the cell membrane marker WGA suggests that reduced cardiomyocyte cell size correlates with elevated *FGF10* levels (**E;** r^2=0.6777, p=0.02). (**F**) For all patients, the proportion of small (<600µm²), medium (600<x<800µm²) and large (>800µm²) cardiomyocytes was determined. (**G**) Elevated *FGF10* levels correlate with low frequency of large cardiomyocyte (>800µm², r^2=0.66, p=0.02). (**H-I**) Histological Sirius red staining showed that elevated FGF10 levels correlate with reduced fibrosis in the border zone (r^2=0.7622, p=0.004). Pictures, according to patient-corresponding FGF10 levels depicted in (A), have been classified from low to high expression as represented by the above grey triangle. Scale bars 100 µm. Statistical significance (p) was determined using Student's *t*-distribution.